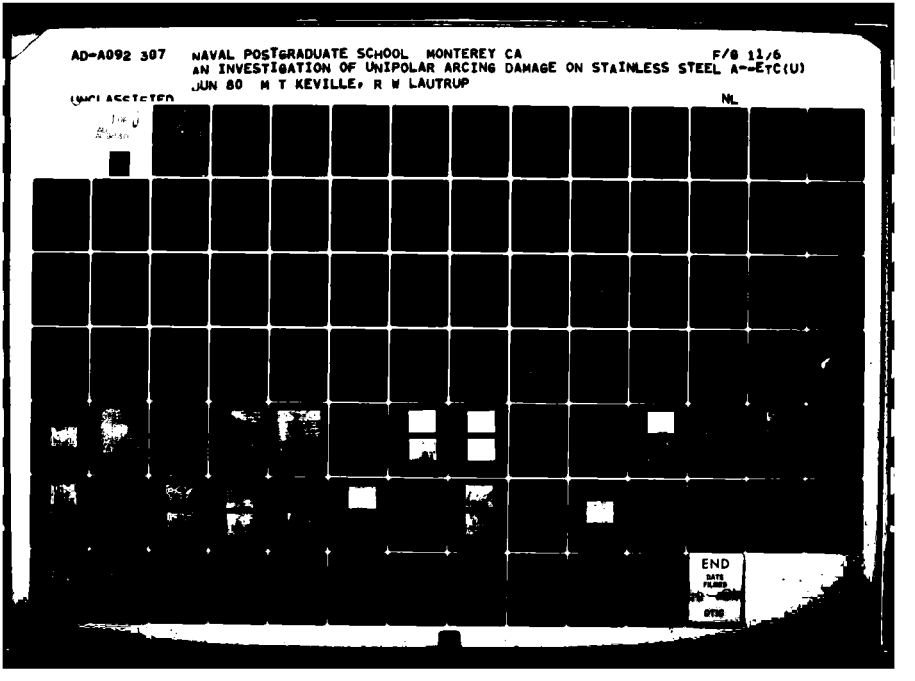
AD-A092 307
NAVAL POSTGRADUATE SCHOOL MONTEREY CA
F/G 11/6
AN INVESTIGATION OF UNIPOLAR ARCING DAMAGE ON STAINLESS STEEL A--ETC(U)
JUN 80 M T KEVILLE, R W LAUTRUP
UNCLASSIFIED
NL
END
DATE FILMED
DTIC

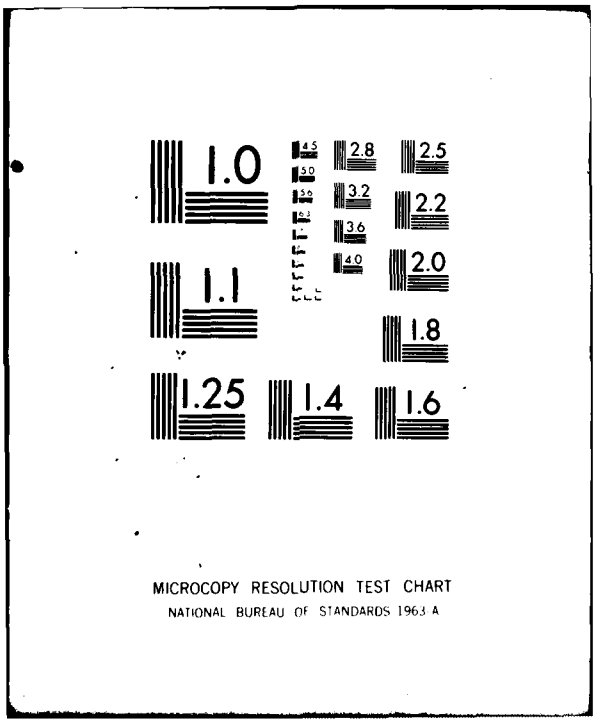
1.0
1.1
1.25
1.4
1.6
1.8
2.0
2.2
2.5
2.8
3.2
3.6
4.0
4.5
5.0
MICROCOPY RESOLUTION TEST CHART
NATIONAL BUREAU OF STANDARDS 1963 A

LEVEL II

(2)

B S.

NAVAL POSTGRADUATE SCHOOL

Monterey, California

AD A092307

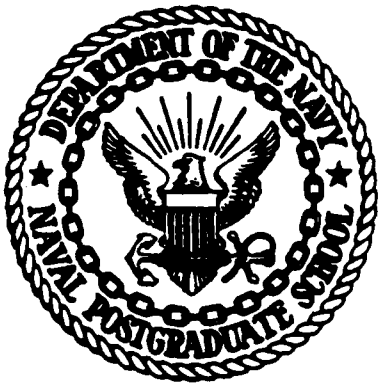

DTIC
ELECTE
DEC 0 2 1980
S D
E

THESIS

AN INVESTIGATION OF UNIPOLAR ARCING DAMAGE ON STAINLESS STEEL AND TITANIUM CARBIDE COATED SURFACES

by

Michael Thomas Keville

and

Robert William Lautrup

June 1980

Thesis Advisors: F. Schwirzke
K.D. Challenger

Approved for public release; distribution unlimited.

DDC FILE COPY

80 12 01 048

UNCLASSIFIED

SECURITY CLASSIFICATION OF THIS PAGE (When Data Entered)

REPORT DOCUMENTATION PAGE	READ INSTRUCTIONS BEFORE COMPLETING FORM
1. REPORT NUMBER	2. GOVT ACCESSION NO. AD-A092307 / 3. RECIPIENT'S CATALOG NUMBER (1)
4. TITLE (and Subtitle) An Investigation of Unipolar Arcing Damage on Stainless Steel and Titanium Carbide Coated Surfaces.	5. TYPE OF REPORT & PERIOD COVERED Master's Thesis; June 1980
	6. PERFORMING ORG. REPORT NUMBER
7. AUTHOR(s) Michael Thomas Keville; Robert William Lautrup	8. CONTRACT OR GRANT NUMBER(s)
9. PERFORMING ORGANIZATION NAME AND ADDRESS Naval Postgraduate School ✓ Monterey, California 93940	10. PROGRAM ELEMENT, PROJECT, TASK AREA & WORK UNIT NUMBERS 61153N
11. CONTROLLING OFFICE NAME AND ADDRESS Naval Postgraduate School Monterey, California 93940	12. REPORT DATE June 1980
	13. NUMBER OF PAGES 92
14. MONITORING AGENCY NAME & ADDRESS(if different from Controlling Office) Naval Postgraduate School Monterey, California 93940	15. SECURITY CLASS. (of this report) Unclassified
	15a. DECLASSIFICATION/DOWNGRADING SCHEDULE

16. DISTRIBUTION STATEMENT (of this Report)

Approved for public release; distribution unlimited.

17. DISTRIBUTION STATEMENT (of the abstract entered in Block 20, if different from Report)

18. SUPPLEMENTARY NOTES

19. KEY WORDS (Continue on reverse side if necessary and identify by block number)

Unipolar Arcs
TiC Thin Film
Plasma Surface Damage
Plasma-Sheath Interactions
Unipolar Arcing Damage Mechanisms

20. ABSTRACT (Continue on reverse side if necessary and identify by block number)

Unipolar arcing was studied using a new method of laser plasma production. The mechanism of unipolar arcing has been shown in the literature to be the most important source of wall erosion and plasma pollution. Arcing is of particular concern in Tokamak nad other magnetically confined fusion devices. The experiment was conducted using a neodymium-glass laser in both normal pulse and Q-switched modes to generate a hot plasma. This plasma, generated from several different targets, was used to initiate arcing on the

DD FORM 1 JAN 73 1473 (Page 1) EDITION OF 1 NOV 65 IS OBSOLETE S/N 0102-014-6601

UNCLASSIFIED 251450

SECURITY CLASSIFICATION OF THIS PAGE (When Data Entered)

#20 - ABSTRACT - (CONTINUED)

surface. From the experimental results, a model of the arcing process was proposed which extended those available in the literature. Further analysis using TiC film deposited by the Activated Reactive Evaporation technique indicated that such films showed promise in preventing or greatly minimizing unipolar arcing damage.

Approved for public release; distribution unlimited.

An Investigation of Unipolar Arcing Damage on Stainless Steel and Titanium Carbide Coated Surfaces

by

Michael Thomas Keville
Lieutenant, United States Navy
B.S., United States Naval Academy, 1974

and

Robert William Lautrup
Commander, United States Navy
B.S., United States Naval Academy, 1964

Submitted in partial fulfillment of the requirements for the degree of

Master of Science in Engineering Science
(Michael Thomas Keville)

Master of Science in Physics
(Robert William Lautrup)

from the

NAVAL POSTGRADUATE SCHOOL
June 1980

Author: Robert W Lautrup

Author: Michael Thomas Keville

Approved by: F. Schwindee
Thesis Advisor

K D Challenger
Thesis Advisor

W E Vincenti
Second Reader

J. R. Dyer
Chairman, Department of Physics and Chemistry

William M. Tolles
Dean of Science and Engineering

ABSTRACT

Unipolar arcing was studied using a new method of laser plasma production. The mechanism of unipolar arcing has been shown in the literature to be the most important source of wall erosion and plasma pollution. Arcing is of particular concern in Tokamak and other magnetically confined fusion devices. The experiment was conducted using a neodymium-glass laser in both normal pulse and Q-switched modes to generate a hot plasma. This plasma, generated from several different targets, was used to initiate arcing on the surface. From the experimental results, a model of the arcing process was proposed which extended those available in the literature. Further analysis using TiC film deposited by the Activated Reactive Evaporation technique indicated that such films showed promise in preventing or greatly minimizing unipolar arcing damage.

TABLE OF CONTENTS

I. INTRODUCTION ---------- 8

II. BACKGROUND AND THEORY ---------- 11

A. UNIPOLAR ARCING ---------- 11

1. Description of the Arcing Problem ------ 11

2. Theory ---------- 13

3. Previous Studies on Arcing ---------- 20

4. Unipolar Arcing ---------- 29

B. THIN FILM DEPOSITION ---------- 32

1. Background ---------- 32

a. Droplet Deposition ---------- 32

b. Atom-by-Atom Deposition ---------- 33

2. Activated Reactive Evaporation Process - 39

a. Description of the Process --------- 39

b. Advantages Gained by Activated Reactive Evaporation ---------- 40

III. EXPERIMENT DESIGN ---------- 43

A. APPARATUS ---------- 43

1. Laser ---------- 43

2. Target Test Chamber ---------- 46

3. Optical Microscope ---------- 46

4. Scanning Electron Microscope ---------- 47

B. PROCEDURES ---------- 47

1. Target Preparation ---------- 47

a. Before Coating ---------- 47

b. TiC Deposition ---------- 49

c. Target Surface Examination --------- 49

2. Plasma-Surface Interaction ---------- 49

3. Surface Damage Investigation ---------- 49

IV. EXPERIMENTAL RESULTS ---------- 51

A. SPUTTERED STEEL COATING ON STAINLESS STEEL DISK ---------- 51

B. STAINLESS STEEL FOIL WITH TiC FILM --------- 59

1. Reference Experiment without TiC Film -- 59

2. Foil Coated with TiC by ARE Process ---- 62

a. Normal Pulse Damage Effects -------- 63

b. Q-Switched Pulse Damage Effects ---- 67

C. STAINLESS STEEL DISK WITH TiC FILM --------- 69

1. Reference Experiment Without TiC Film -- 69

2. Disk Samples Coated with TiC by ARE Process ---------- 74

V. DISCUSSION ---------- 78

A. THE PROCEDURE ---------- 78

B. CONDITIONS THAT PROMOTE UNIPOLAR ARCING ---- 78

C. INITIATION OF UNIPOLAR ARCING ---------- 79

D. CRATER FORMATION ---------- 80

E. ARC CESSATION ---------- 81

VI. CONCLUSIONS ---------- 84

BIBLIOGRAPHY ---------- 86

INITIAL DISTRIBUTION LIST ---------- 92

ACKNOWLEDGMENT

We wish to thank Robert Sanders, whose technical assistance in the laboratory, and continuing support made our thesis possible. We are also particularly grateful to Thomas Kellog who guided and supported our work in the material science laboratories. We would also like to express our gratitude to Professors F. Schwirzke and K.D. Challenger for their help and guidance throughout this thesis and particularly for their willingness to work together on an inter-disciplinary thesis. Professor K. Woehler freely contributed by his careful review of our work. Professor R. Bunshah of UCLA provided the coated samples that we needed. Judy Cooper was extremely helpful in the administrative area.

Most of all, we want to thank our Lord, who made it all possible.

I. INTRODUCTION

Confined fusion energy sources have become the focus of significant scientific and technological effort as the limits of fossil fuel reserves have been recognized. In the past decade significant theoretical advances and parallel technological progress have brought fusion power much closer to operational reality. However, there are still difficult problems to be overcome. The phenomena of plasma-surface interactions have led to many difficulties in this field. The products of these interactions are undesirable plasma impurities which ultimately result in the inability to establish a self-sustaining plasma. Another problem to be solved is the damage to walls caused by thermalization of high energy neutrons. This study was focused on the more immediate of these two problems, that of plasma-surface interactions.

The primary damage effects of the plasma-surface interaction are sputtering, evaporation, and unipolar arcing. The physical process involved in sputtering is predominantly a momentum transfer process. When an energetic ion or neutral atom strikes a solid surface, a collision cascade with the lattice atoms is produced. When this cascade results in a surface atom receiving sufficient energy to exceed the binding energy, sputtering results [37]. Evaporation is primarily caused by absorption of radiant heat at the wall surface.

Evaporation is a well known process that can be predicted quite accurately given the wall composition, the equilibrium vapor pressure curves for the material, and knowledge of the surface temperature as a function of time. Unipolar arcing is a phenomenon whereby an arc is established between a hot dense plasma and a conducting wall, with the wall acting as both the cathode and the anode. These arcs have been reported in recent studies as the most significant among the three damage mechanisms [19,43].

Several methods of inhibiting these interaction phenomena are currently being developed. Included in these efforts are improved surface preparation; optimization of wall material and configuration; and special emphasis given to the development of "hard" and sputter resistant wall surfaces.

An advanced deposition technique, Activated Reactive Evaporation (ARE), was developed by Bunshah [7]. The films deposited by this process appeared to have significant advantages over those from other processes. The study reported by this thesis was an investigation into the effectiveness of thin films of titanium carbide deposited by ARE in eliminating unipolar arcing.

A pulsed laser was used to generate a plasma over the surface of the samples and damage was assessed using both optical and scanning electron microscopy, and x-ray analysis techniques. As background to this study, the theory of arcing phenomena in general, and unipolar arcing in particular,

were considered in detail. The development and characteristics of various techniques of thin film deposition were likewise investigated in some depth.

The results of this study have shown that thin films of titanium carbide may indeed be capable of solving the unipolar arcing problem.

II. BACKGROUND AND THEORY

A. UNIPOLAR ARCING

1. Description of the Arcing Problem

The problem of interaction between hot plasmas and hard surfaces has been of interest since the beginning of power generation fusion programs, and the resulting research on plasma confinement devices. This interest has increased recently as realistic designs for confining fusion plasmas are being tested operationally.

There are two major reasons for this concern. First is the damage to the first wall itself by the plasma; and second, damage interaction products which introduce impurities into the plasma. Unipolar arcing, because of the small scale of physycial erosion, has not been of primary structural concern, but is rather a problem encountered in seeking to achieve sustained, magnetically confined fusion [36]. The products of plasma-surface interactions contaminate the plasma resulting in radiation losses from high atomic number, Z, particles, which causes sufficient cooling that the plasma can not be sustained at fusion temperature [36,54,55].

In order to support this type of research, there has been a parallel effort to develop better plasma diagnostic techniques, to determine the actual values of reaction parameters such as magnetic fields, currents, voltages, temperatures,

and the presence of specific phenomena such as arcing within plasma. The detailed information obtained by these diagnostics has resulted in more precise theoretical models which are useful in obtaining a better understanding of problems such as unipolar arcing. Through these models the relative importance of plasma pollution mechanisms has been determined in a quantitative manner [19].

One of the important results of recent research is that surface erosion due to evaporation and sputtering, while remaining of significant importance of themselves, are shown to be greatly increased in the presence of unipolar arcing [23,2]. More significantly, it has been experimentally shown that the erosion of stainless steel due to unipolar arcing is two orders of magnitude greater than sputtering in DITE and Russian Tokamaks [36,43]. Tests have been conducted in the Columbia University shock tube device; producing a hot, dense deuterium plasma closely simulating the conditions of a toroidal confinement machine. These tests have demonstrated that arcing would cause most significant problems under the conditions present in an operational fusion power reactor [61].

Unipolar arcing was first observed many years ago [51] and was proposed to be the source of metal impurities in diffuse pinches. More recently it has been observed and described extensively by a study conducted at DITE by Goodall and McCracken [19]. The study provides firm physical evidence

that unipolar arcing does occur on test probes, limiters, and the first wall itself; and that this damage mechanism is the dominant one. The study concludes that "... arcing is consistent with all the experimental evidence concerning the behavior of metals in Tokamak discharges. Not only the quantity of metal, but also the variation of concentration as the low Z impurity is changed or as hydrogen is puffed in, are all consistent with arcing."

As a result of the increasing evidence indicating the dominance of unipolar arcing as a damage mechanism in plasma surface interactions, the study reported by this thesis was focused on determining experimentally the effectiveness of thin films of stochiometric TiC in reducing unipolar arcing between a laser generated plasma, and a stainless steel substrate.

2. Theory

A plasma is defined as a quasi-neutral gas of charged particles which exhibits a collective behavior. A fundamental characteristic of a plasma is its ability to shield out electric potentials applied to it. The characteristic shielding length of a plasma is the Debye length (λ_D) where

$$\lambda_D = \left(\frac{k T_e}{4 \pi n e^2}\right)^{1/2} \qquad (1)$$

where:

k = Boltzman constant

T_e = electron temperature

n = plasma density

e = electron charge

In order for shielding to exist, and for the sheath to exist and for the plasma to act collectively, a sufficiently large number of electrons and ions must be present. The number of particles in a Debye sphere (N_D) is given by:

$$N_D = \frac{4}{3} \pi n \lambda_D^3 = 1380 \frac{T^{3/2}}{n^{1/2}} \text{ [T in °K]} \quad (2)$$

For a plasma $N_D >> 1$. A gas in thermal equilibrium has particles of all velocities present. The most probable distribution of the velocities, u, at equilibrium is the Maxwellian distribution:

$$f(u) = A \exp\left(-\frac{1}{2} \frac{m u^2}{k T}\right) \quad (3)$$

where:

m = mass of particle species.

This leads to the fact that the average energy per particle per translational degree of freedom is given by

$$E_{av} = 1/2\,k\,T \qquad (4)$$

As a convention, temperature of a plasma is expressed in terms of electron volts where a temperature of 1 ev = 11,600 °K.

Because of the difference in charge and relative mass, the ion temperature (T_i) does not necessarily equal the electron temperature (T_e) within the plasma. Since interaction rates are different, the electrons and ions may be in thermal equilibrium within their own species but not have time to be in thermal equilibrium with the other species.

If the electron leakage from the plasma to the wall (divertor, probe, etc.) is more rapid than the ion leakage, the plasma takes on a positive potential relative to the wall. Due to the relative mass differences, the electrons have much higher thermal velocities. Thus, this situation of more rapid electron leakage is a common condition for a plasma [39].

The function of the sheath is to establish a potential barrier so that the more mobile species, usually electrons, are confined electro-statically [7]. The plasma potential will build up to the level where ion losses match electron losses, thus maintaining plasma neutrality [7,39].

Figure 1 illustrates the Coulomb barrier in a sheath, reflecting electrons.

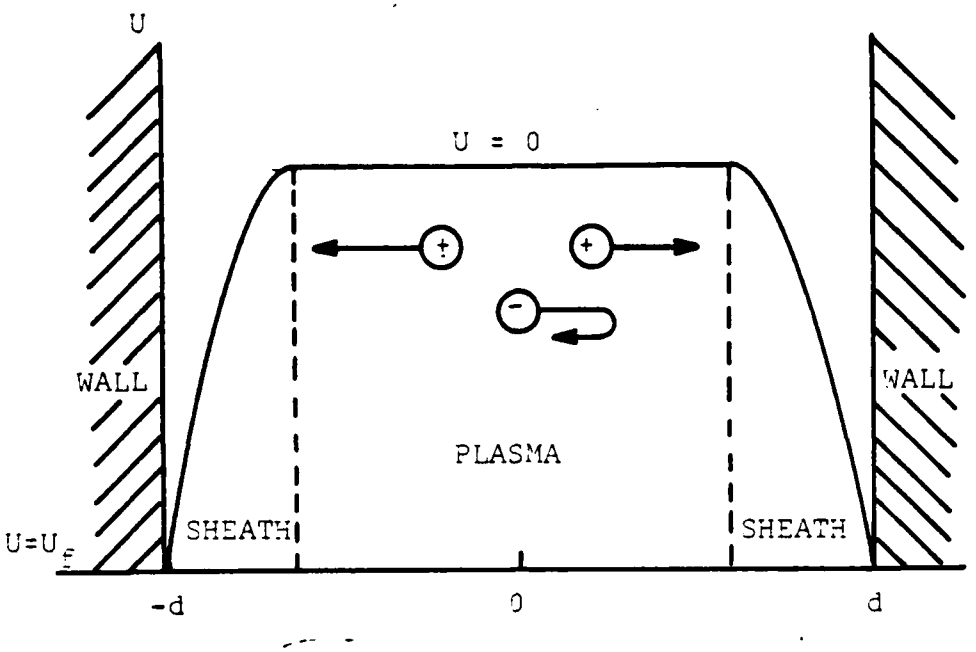

Figure 1. Plasma potential and sheath

The foregoing discussion describes the well-known Langmuir sheath condition.

The electric field, E, in the sheath, between a plasma and the surface is of the order:

$$E \tilde{=} \frac{-U_f}{\lambda_D} \qquad (5)$$

where:

U_f = the floating or sheath potential.

$$U_f = \frac{k\,T_e}{2\,e} \ln \frac{M_i}{2\pi m_e} \qquad (6)$$

where:

T_e = electron temperature

e = electron charge

M_i = ion mass

m_e = electron mass

Only the electrons in the high energy tail of the Maxwellian distribution can overcome the sheath potential. Ions entering the sheath are accelerated and gain energy. Since the ions are much more effective than electrons in sputtering and the sputtering rate for deuterons increases steeply with energy in the range of $10^2 - 10^3$ eV, sputtering and desorption of loosely bound metal atoms [56] will become worse if the sheath potential increases due to an increase of electron temperature near the wall [49].

Consequently, large influxes of metal atoms are observable during Tokamak disruptions and wave and beam heating experiments. In each of these cases a higher temperature plasma is contacting the wall.

Unipolar arcing occurs if the sheath potential increases enough to sustain an arc [36,40]. Electrons are then emitted from a surface spot into the plasma. This reduces the nearby plasma potential and less energetic electrons

from the high energy tail of the Maxwellian distribution can reach the wall, thus closing the current loop. In the arc, the ion current magnitude, J, is determined from the Child-Langmuir law of space charge limited current:

$$J = \frac{4}{9} \left(\frac{2\,e}{M_i}\right)^{1/2} \frac{|U_f|^{3/2}}{4\,\pi\,d^2} \qquad (7)$$

where:

e = electron charge

M_i = ion mass

U_f = floating potential

d = distance

Figure 2 illustrates the potential distribution and fields present near a cathode spot. What causes the initial breakdown and the formation of the cathode spot is still under discussion.

The minimum requirement for the onset of unipolar arcing is that the sheath potential is comparable to the ionization energy. The ionization energy (U_i) of Fe is 7.9 eV and that for Cr is 6.8 eV [54]. The sheath potential for the Fe-plasma is

$$U_f = 4.83 \frac{k\,T_e}{e} \qquad (8)$$

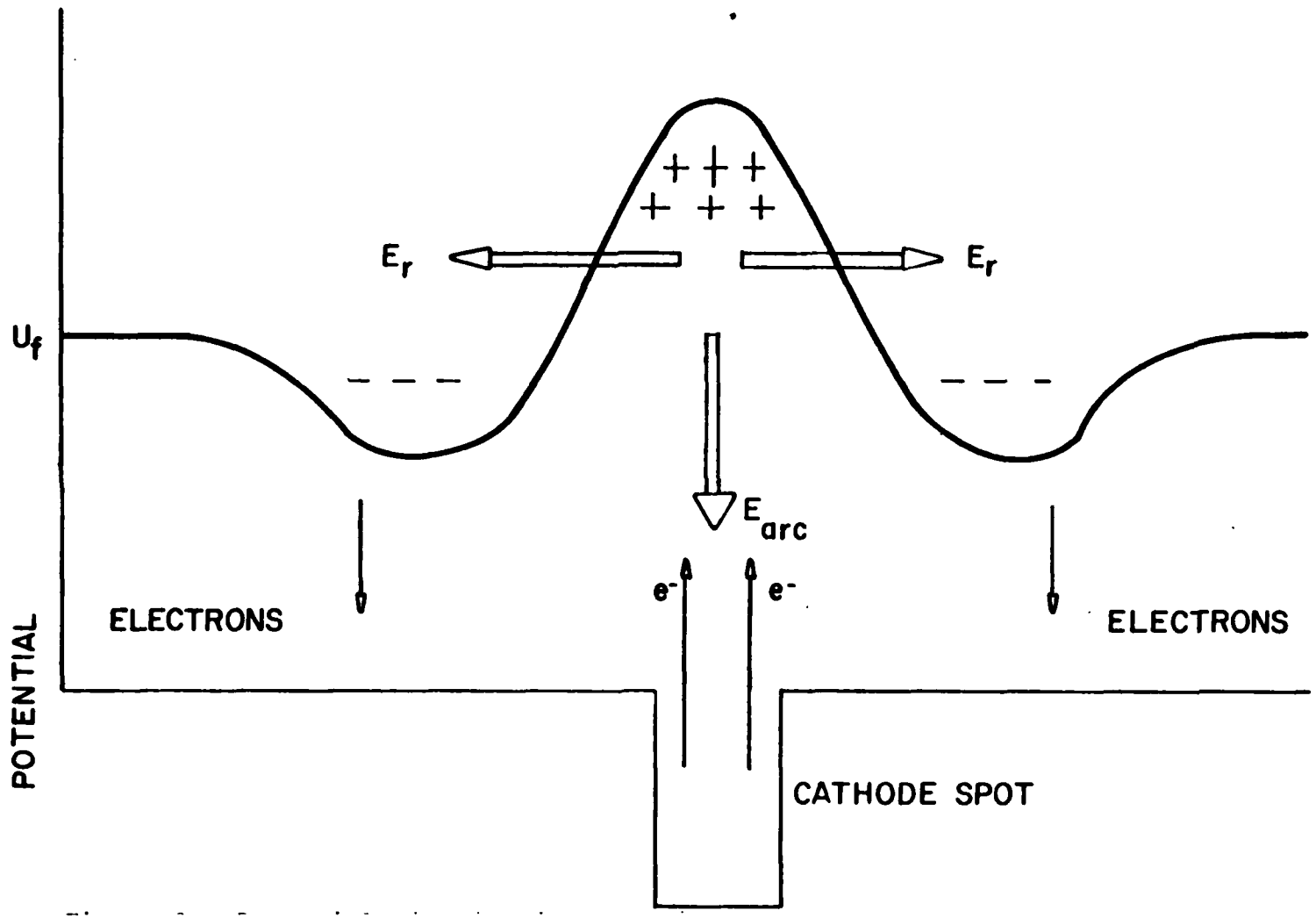

Figure 2. Potential distribution at unipolar arc.

Thus the minimum electron temperature for the onset of arcing in stainless steel is about kT_e = 2 eV. The binding energy of Fe is about 4 eV which is about half of its ionization energy.

For an arc to develop it is also necessary that the ion density increase above the cathode spot, in order to enable a larger electron current to flow into the plasma.

The increased electric field strength on the wall surface, caused by collection of charges at surface protrusions, will increase the ion flux from the plasma to these spots. Surface protrusions are considered relative to the average surface smoothness and may be metallurgical inhomogeneities, inclusions, or whiskers from processing operations, such as milling and grinding.

Increased ion bombardment and recombination rates lead to locally increased surface temperature. This increase in local temperature results in ejection of neutrals from the surface into the plasma sheath. Ionization of the neutrals results in a local increase in density of the plasma above the cathode spot and an arc is established which continues to remove material from the spot.

A more complete description of the unipolar arcing process is discussed in the conclusions of this thesis.

3. Previous Studies on Arcing

Unipolar arcing is a serious problem which must be overcome to achieve successful operation of a fusion power

reactor. The efforts to solve this problem have taken on new significance as existing fusion test facilities report having confined a plasma to within approximately one decade of the well-known Lawson criteria. Other facilities have achieved temperatures greater than sixty percent of that required for break-even.

"Hard" metals like molybdenum and tungsten have low sputtering rates at deuteron energies of 10 - 100 eV. However, those high-Z materials radiate very strongly in a fusion-like plasma and only a very small concentration can be tolerated. This is the "crux" of the unipolar arcing problem; unipolar arcing has been shown to be two orders of magnitude more important than sputtering in the introduction of high-Z impurities into a plasma [43].

A. E. Robson and P. C. Thoneman were the first to study and report on the subject of unipolar arcing [51]. Their experimental work used a tube which had a mercury electrode in the presence of a plasma generated by an electrodeless high-frequency discharge. The tube was evacuated to a pressure of less than 10^{-6} Torr. The mercury vapor pressure at room temperature is 1.76×10^{-3} Torr. An arc was initially established with an external anode voltage applied. Thus the plasma was generated. As the plasma density was increased, the arc current increased. When the external supply to the anode was turned off, the arc remained in the unipolar mode. As the plasma density produced by the R. F. pumping was

reduced the arc continued until it vanished when plasma density became too low to sustain it.

Robson based his theoretical discussion on the floating potential derived from the works of Langmuir and Bohm. He said that with the wall at the floating potential, U_f:

$$U_f = \frac{k\,T_e}{2\,e} \ln \frac{M_i}{2\pi\, m_e} \qquad (6)$$

where:

e = electron charge

m_e = electron mass

M_i = ion mass

T_e = electron temperature

if the electron temperature is sufficiently high, the floating potential will exceed the potential required to sustain an arc. If under these conditions a cathode spot is initiated, the strong emission from the spot will reduce the potential from the wall to plasma from U_f to U_c (cathode fall potential). More electrons can now reach the wall from the plasma against the reduced retarding potential except at the small cathode spot. The arc current flows to the wall and returns through the cathode spot. The circulating current was calculated to be:

$$I_c = A\, n\, e\left(\frac{k\,T_e}{2\pi m_e}\right)^{1/2} \left\{\exp\left(\frac{-e\,U_c}{k\,T_e}\right) - \exp\left(\frac{-e\,U_f}{k\,T_e}\right)\right\} \quad (9)$$

where:

A = area of the plate exposed to the plasma.

The conclusions were that there is a critical plasma density and electron temperature required in order for a unipolar arc to exist but also there must be some mechanism by which the arc is initiated such as ion heating of the wall. Figure 3 shows the two conditions for the sheath potential with and without unipolar arcing as Robson described.

Early arc studies with various metals, in the absence of an imposed magnetic field, showed that for easily vaporizable metals the arc tended to be stationary [10,31]. It was also noted that the arc was initiated due to the establishment of fields which resulted from minute impurities within the metal or the presence of thin insulating areas on the cathode surface. Also observed was that many arc reactions resulted in the phenomenon of vapor jet erosion from the cathode. As a result of these studies the vapor jet velocity was shown to be a unique function of the vapor production per unit surface area and the vapor density [31]. Calculated and observed velocities were found to be in agreement and of the order of 10^5 cm/sec.

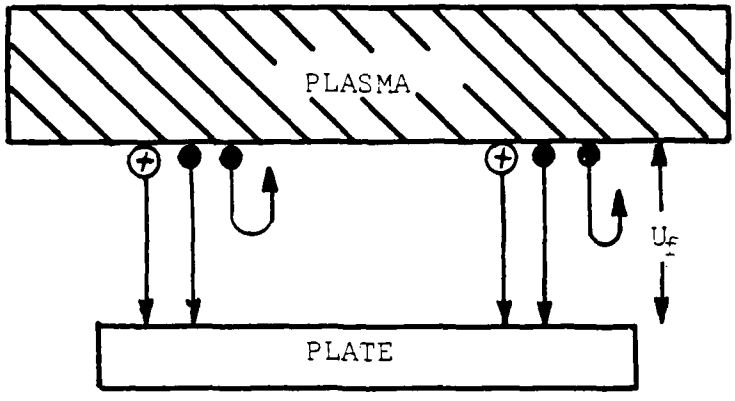

⊕ ION ● ELECTRON

Figure 3a. Equilibrium of isolated plate with no cathode spot.

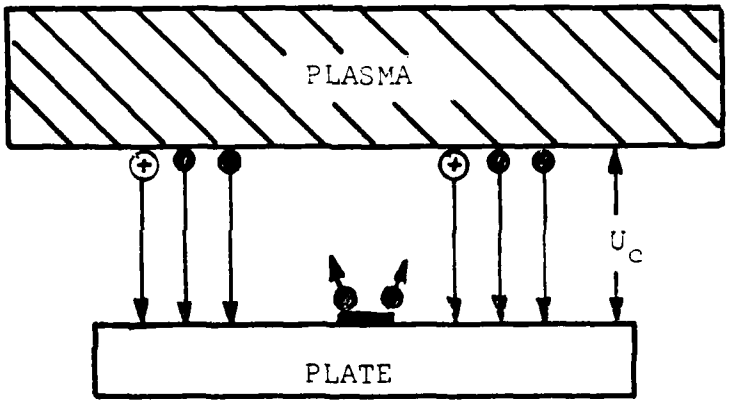

⊕ ION ● ELECTRON

Figure 3b. Equilibrium of isolated plate with a cathode spot.

Erosion measurements on copper cathodes have shown the erosion rate to be primarily dependent on arc current, arc duration and cathode size. The behavior of other cathode metals was found to be similar [10]. In a vacuum discharge, charged and neutral particles are present. For cathodic arcs, i.e., where there is no anode spot, neutral particles are emitted from the cathode surface, and a fraction becomes ionized in the nearby plasma.

While these studies were based primarily on work with copper cathodes and millisecond arcs, the results are of significance to unipolar arcing since arcs with a lifetime as short as 100 nanoseconds were investigated.

A validated conclusion based on these studies indicated that the mechanism of ion production is not altered by the arc duration or cathode area [45].

Continued work in the area of direct current vacuum arcs established that the current is of the order of 10 - 50 amperes [12]. Ion velocity estimates were further refined to 10^6 cm/sec. It was postulated that initially many neutral atoms and low energy electrons are emitted from the cathode. Those electrons gain energy from the electric field. Ionization of neutrals begins when the average electron energy is a few electron volts. Ionization results from two distinct processes: (1) the higher energy electrons ionize atoms directly in single collisions, and (2) because of very great densities of both electrons and neutrals just above the cathode

spot, an atom can be ionized by a series of inelastic collisions, with the time between collisions being less than the lifetime of the excited atom in its particular energy state. A peak of positive ion concentration is formed near the cathode. Quasi-neutrality requires a coincident local electron maximum. However, the thermal electron velocity is much higher than that of the ion. As a consequence electrons tend to flow out of the region of production much more quickly. This results in a net local surplus of positive ions which creates a maximum positive potential (hump) in the region. The electrons are slowed by the resulting electric field (see Figure 4) and the positive ions are accelerated until the charge loss rates of ions and electrons are equal (i.e., an ambipolar diffusion controlled process). This potential hump increases in magnitude as long as the local plasma density increases due to ionization of neutral particles. Figure 4 shown below shows the proposed potential distribution. The potential gradient is determined as follows:

(a) $$e\, n\, E = -\nabla P \tag{10}$$

where:

∇P = plasma pressure gradient

(b) $$E = \frac{-k\, T_e}{e} \frac{1}{n} \frac{dn}{dx} \tag{11}$$

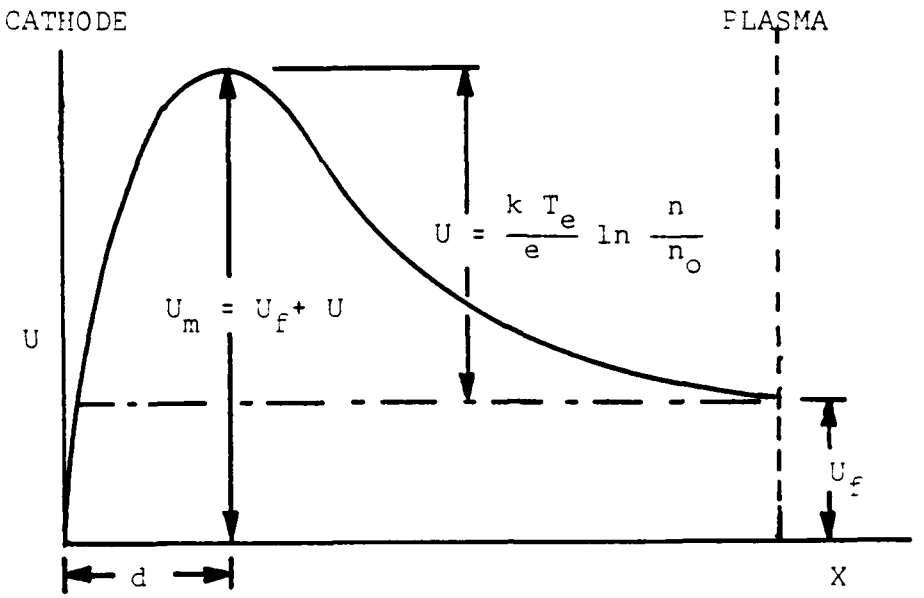

Figure 4. Assumed potential distribution in a vacuum arc (U_a = arc voltage)

$$\text{(c)} \qquad E = \frac{-dU}{dx} \tag{12}$$

eliminating the dx terms;

$$\text{(4)} \qquad \int_{U_f}^{U_c} dU = \frac{k T_e}{e} \frac{1}{n} dn \tag{13}$$

$$\text{(e)} \qquad \Delta U = U_c - U_f = \frac{k T_e}{e} \ln \frac{n}{n_o} \tag{14}$$

This theory of the potential hump explains the observed occurrence of high energy ions (40 - 80 eV). It was implied that the density of ions must decrease very rapidly away from the potential hump region.

A study by E. Hantzsche, et al., [21], reported extensively on the erosion of metal cathodes by arcs. This work primarily dealt with nanosecond pulse breakdowns. It was established that the initiating micropoints (cathode spots) have a dimension of 10^{-6} meter. The plasma produced at the copper cathode spot expanded at a rate of 2×10^{6} cm/sec and had an energy of approximately 85 eV. It was also shown that the electron emitting point which causes an arc is destroyed in the process; but as a result of the arcing new sites appear. The arc rim may serve as a new point where a stronger electric field exists. Also, some of the numerous droplets of metal which were observed to form at the arc and disperse radially about the cathode spot, produce new micro-inhomogeneities and new field emitting points which are potential arcing sites.

Another important conclusion of the Hantzsche study was reached concerning the mechanism of destruction and production of emitting sites. There is a smoothing of the surface micro-roughness by local melting if the arcing period is less than the heat transfer period. After such smoothing a greater arc initiation voltage is required. On the other

hand, enlargement of roughness and crater formation lead to a decrease in the breakdown voltage if heat transfer is significant.

It has been demonstrated that arcing and vacuum breakdown mechanisms are very similar [21]. Hantzsche also concluded that if the current $i > 5 \times 10^{12}$ A m^{-2}, the heat conduction in the material is insufficient to allow a stationary top temperature of the protrusion. It was also concluded that if $i > 7 \times 10^{13}$ A m^{-2}, the protrusions will explode due to local pressure, thus producing a smoothing effect.

Kimblin, who continued the work with long period vacuum arcs in order to develop a predicting model for erosion rates, confirmed earlier arc current measurements for a variety of materials, but did not attempt to study the cathode process itself [31].

4. Unipolar Arcing

Unipolar arcing requires the presence of a plasma near a conducting surface. A net negative charge with respect to the plasma will be established on the surface (wall) due to the fact that electron flux and ion flux must be equal. If the potential that is established exceeds a critical voltage (~10 V dc) low impedance cathode spots will form [61].

A widely referenced explanation for unipolar arcing by Miley [39] is illustrated in Figure 5. In this theory it is assumed that the plasma takes on a positive potential

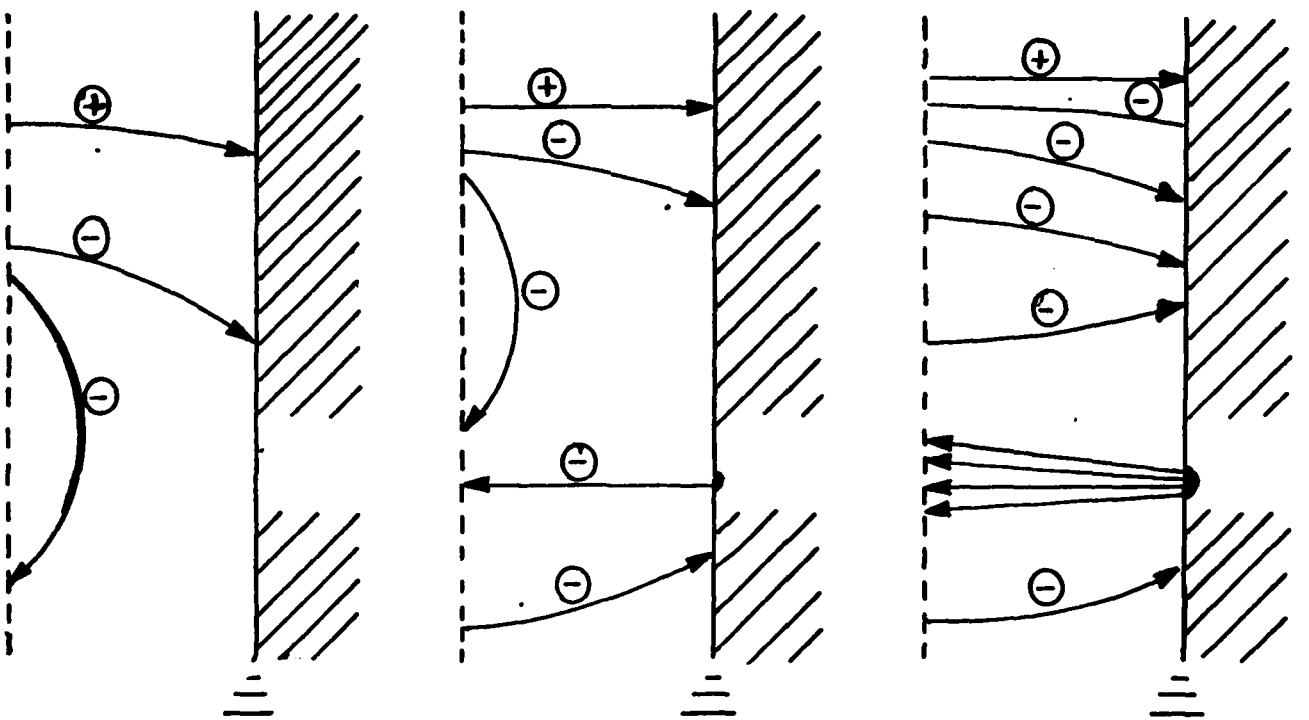

Plasma with no arc Plasma arc initiating Unipolar arc

Figure 5. Formation of a unipolar arc (Miley)

relative to the surrounding wall. This explanation expands Robson's work and is based on the well-known description of the Langmuir sheath. When unipolar arcing occurs ion bombardment from the plasma creates local hot spots on the wall. The hot spots emit electrons from the wall which flow back into the plasma. This electron flow is equivalent to an outward flow of ions. The plasma potential falls below the original value, which allows larger electron leakage currents to flow from the plasma. Ultimately a balance is set up with this increased electron current from the hot spot. This phenomenon has been called unipolar arcing because the wall serves both as the anode and cathode.

Miley's model and conclusions have been substantiated by others [43]. Dealing particularly with the Tokamak, it was calculated that the theoretical plasma pollution from unipolar arcing should be one hundred times as great as from sputtering, which has been confirmed, as mentioned previously.

A diagnostic method utilizing a double probe has been developed [30] to detect the presence of unipolar arcing. This technique and efforts in the spectroscopic area [52] have provided new information useful in the effort to find a means of suppressing unipolar arcing. The assessments of this thesis were limited to after-the-fact analysis by optical and scanning electron microscopy.

B. THIN FILM DEPOSITION

1. Background

The deposition of films of material on a substrate is a process that has been in use for many years. The early applications of adhesive thin films were mainly decorative, or for mechanical strengthening. During the last two decades, the interest in mononitrides, carbides and oxides of the transition metals of group IV to VI of the periodic table has increased substantially because of their unique combination of properties [13].

Thin films of these materials display many desirable characteristics including increases in hardness, melting temperature, corrosion resistance, abrasion resistance, electrical conductivity, and chemical inertness. These properties, and combinations of them produce a broad spectrum of possible applications for thin film technology [8]. Methods of deposition may be placed in one or two general classifications, droplet transfer, and atom-by-atom transfer.

a. Droplet Deposition

The more common examples of droplet deposition are plasma spraying, flame spraying, detonation gun coating, arc spraying, and wire explosion spraying. Coatings deposited by these methods result in significant surface porosity which is a serious flaw for applications involving plasma-surface interaction.

These processes are characterized by molten or solid "chunks" or droplets of the coating material which are forced onto the substrate surface, impinging on the surface with sufficient kinetic energy to embed the droplet in the surface, as with detonation gun coating; or with a combination or high thermal and kinetic energy, as with flame spraying, which results in adhesion to the surface [5,37]. Porosity is a consequence of both the condition of the substrate, and the stresses developed between droplets. In addition, these processes do not have the surface preparation advantages of many atom-by-atom deposition techniques which remove oxides and other surface inclusions as a result of atomic particle bombardment of the surface [46]. Droplet techniques often result in the entrapment of these surface impurities which increase the porosity and reduce adhesion to the surface.

The advantage of the droplet techniques, for applications that are not critically sensitive to surface porosity, is the simpler coating procedures and correspondingly lower cost [37]. The widespread commercial use of droplet deposition techniques is evidence of the great utility of these processes.

b. Atom-by-atom Deposition

Processes which deposit coatings through an atom-by-atom transfer include physical vapor deposition (PVD), chemical vapor deposition (CVD) and electro-deposition. Among

these methods there are significant differences in the control of the two basic steps of the deposition process. These steps are formation of the species to be deposited and growth of the deposit after condensation. In CVD and electrodeposition these steps take place simultaneously. In the PVD process these steps are essentially independent of each other resulting in more control over the parameters which govern these steps. With these added controls the growth rate of crystal structure may be specified as well as the substrate temperature, which ultimately determines the microstructure and mechanical properties of the deposit [7].

Although there are many different geometric configurations in use, these are included in basically three primary PVD processes: evaporation, ion plating, and sputtering.

The evaporation process is normally carried out in a vacuum. In this process a vapor of the source material is produced by a method such as electron beam heating. The vapor is then transported by line-of-sight to the substrate material. The process is pictured in Figure 6, taken from Reference 7.

The ion plating process is similar to that of evaporation with the addition of an inert gas glow discharge, usually argon, interposed between the source material and the substrate. Figure 7 is a schematic of this configuration [7]. The discharge is produced by charging the substrate

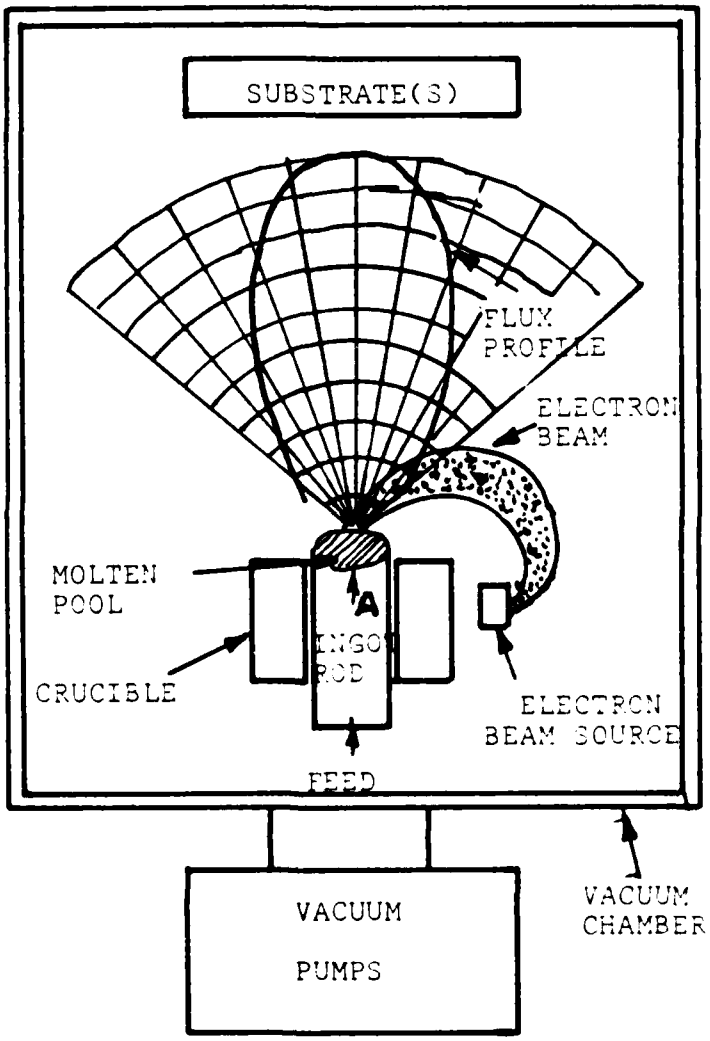

Figure 6. Vacuum-evaporation process using electron beam heating.

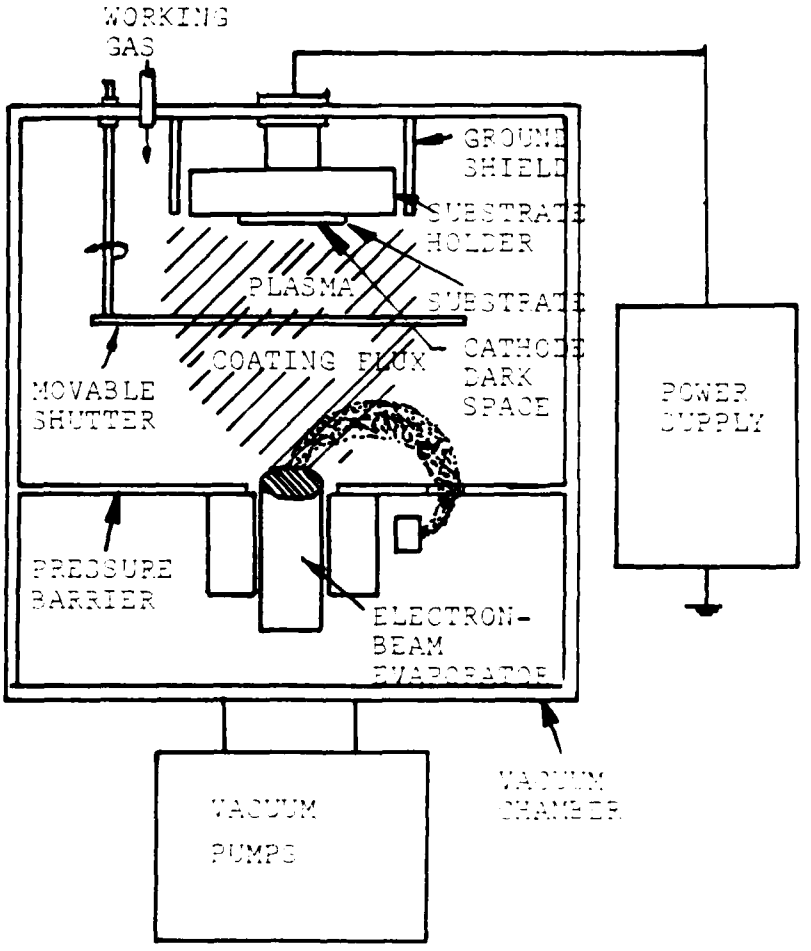

Figure 7. Ion-plating process.

to a high negative potential (2 to 5 kV). The substrate is bombarded with the ions which provides a constant cleaning effect, resulting in improved adhesion. The primary improvement that this provides over simple evaporation is the even coating produced as the discharge gas ions collide with the coating vapor atoms causing an even spread.

The sputtering process, as shown in Figure 8, also uses a glow discharge; however in this method the discharge ions impinge upon the target source material directly. Groups of atoms are sputtered off the target by this momentum transfer process and are vaporized in the discharge prior to deposition on the substrate.

The PVD processes result in several advantages which are outlined by Bunshah as follows [7]:

1. Production of simple shapes (sheet, foil, or tubing) directly, of full density, from metals, alloys, and ceramics at high deposition rates (0.001 in/min or 250,000 A/min), which is a very important economic consideration.

2. Very high purity of deposits.

3. Very fine grain size (~1 μm) in the deposits, thus increasing the strength with toughness as contrasted to other methods of strengthening, such as solid solution or precipitation, where strength is increased at the expense of toughness.

4. Growth of single-crystal deposits on seed crystals.

5. Excellent bonding to the substrate in systems where metallurgical bonds can be formed.

6. Surface finish equal to that of the substrate, thus minimizing or eliminating post deposition machining or grinding. Conversely the defects in the surface finish of the substrate will also be replicated in the deposit.

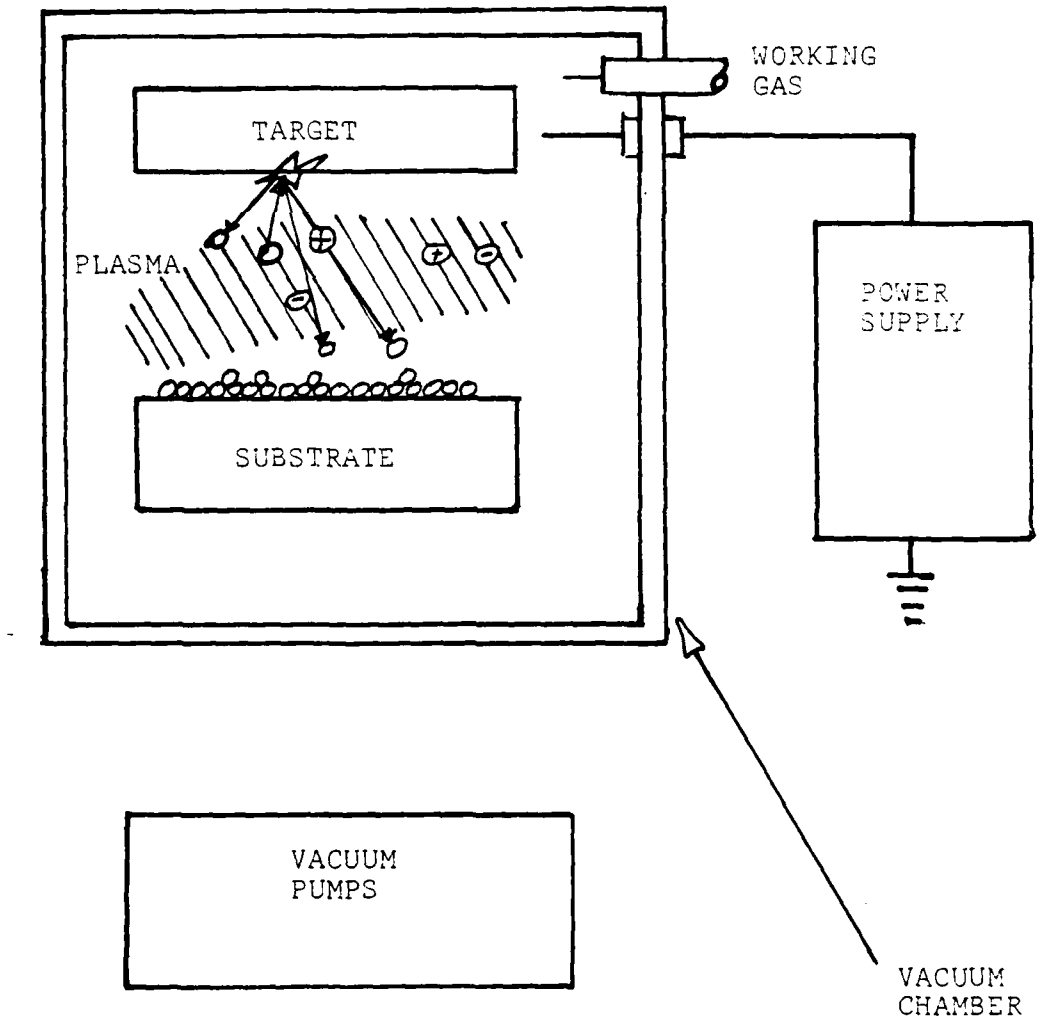

Figure 8. Schematic of sputtering process.

These advantages are well documented and have been confirmed by other studies [8,20,32]. Clearly there are many benefits to be gained by employing these methods of thin film deposition for the solution of metallurgical problems where use of films is deemed appropriate.

The primary weakness of the PVD techniques is that evaporated source atoms striking the surface often adhere to a position where the binding potential is a local minimum. Depending on the effective binding energy, thermal motion can cause desorption or migration of the adatoms to sites where they are more tightly bound. Consequently the micro-structure of the coating depends on the surface mobility of the adatoms which is determined by the temperature of the substrate and the kinetic energy of the incoming atoms. The effect of the limited mobility on the overall coating process is a less tightly bound film, a reduction in the rate of deposition, and variation in the composition of the coating [5].

2. Activated Reactive Evaporation Process

a. Description of the Process

Among the physical vapor deposition (PVD) processes, activated reactive evaporation has been shown to be particularly effective in coatings of the transition metal mononitrides, -oxides, and carbides. In the ARE process, the problems mentioned above for other PVD processes have been significantly reduced. The process is shown in

Figure 9 as developed by Bunshah [7]. In this process, metal or alloy vapors are produced in the presence of a reactive gas such as C_2H_2, which is activated by the glow discharge produced by biasing voltages. This technique produces a quicker and more stochiometric reaction due to ionization of both gas and metal atoms for a reaction such as [8]:

$$2Ti + C_2H_2 \rightarrow 2TiC + H_2$$

The process initiates by heating the source metal with an electron beam at a high acceleration voltage. The molten pool develops a plasma sheath at the surface of the source. The lower energy secondary electrons are pulled from the plasma sheath into the reaction zone by an electrode placed above the surface and biased to a low positive dc potential (20 - 100V). The 100 eV electrons have a high probability for ionization of neutral atoms. In addition, by varying the partial pressure of the reactant gases the metal-to-carbon ratio of the coating can be adjusted in either direction.

b. Advantages Gained by Activated Reactive Evaporation

The flexibility gained by variable substrate temperature and control of reactive gas pressures in the ARE process produce significant improvements in surface quality

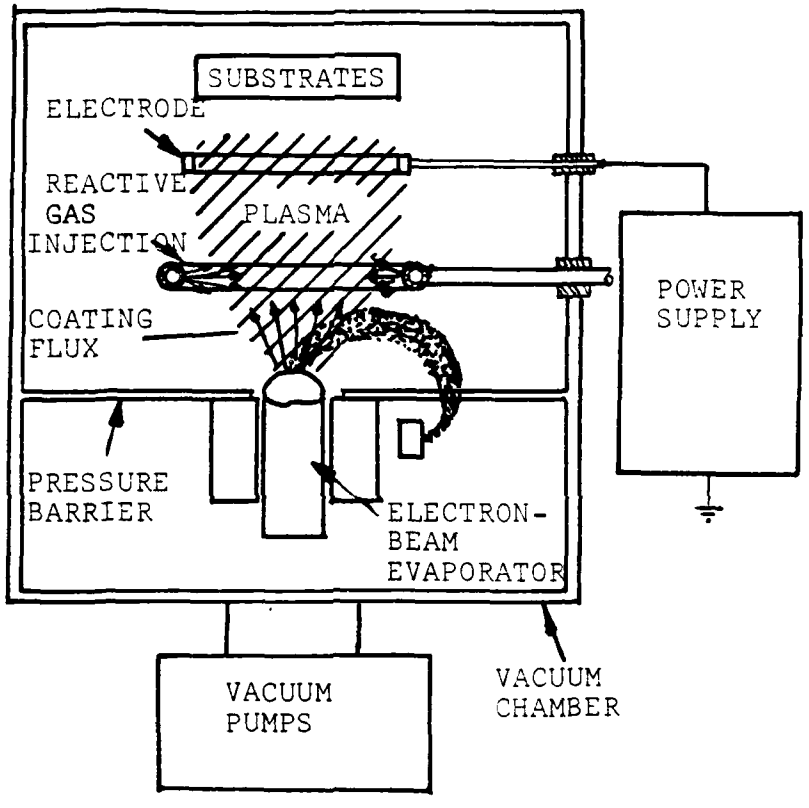

Figure 9. Schematic of the activated reactive evaporation process.

of the deposited film. The substrate temperature has a direct effect on the mobility of adatoms which attach to the surface at a point of low binding potential. If the temperature is insufficient for the adatom to be thermally moved to a point of stronger binding potential the coating can have poor adhesion. Thus by independently raising the temperature of the substrate the adhesion of the coating can be improved without reducing the rate of deposition or adjusting the metal-to-carbon ratio [7].

The substrate temperature control, in addition to improved adhesion, results in direct control of grain size and other microstructural properties [7,8]. Since these microstructural properties directly influence other characteristics of the coating, such as conductivity and hardness [3], many advantages are realized as a result of controlling this variable.

The metal-to-carbon ratio, which is controlled by the partial pressure of the reactive gases, also has great influence on the characteristics of the TiC film. The ARE process consistently results in a higher carbon-titanium ratio [32,59] which enhances those properties of the coating desirable in a hot plasma environment; higher melting temperature and greater thermal conductivity results in less evaporation and reduced localization of heat which should reduce the probability of arcing. Improved adhesion of the coating is critical to the reduction of wall sputtering.

III. EXPERIMENT DESIGN

A. APPARATUS

The apparatus used for this experiment included a neodymium glass laser and an evacuated target test chamber. An optical microscope, a scanning electron microscope, and an energy dispersive x-ray analyzer were used to study the samples. The laser was used to irradiate type 304 stainless steel targets with varied surface preparations, which were mounted in the test chamber. Figure 10 is a schematic of the laser and the test chamber arrangement. The optical and scanning electron microscopes were used to characterize the surface conditions of the targets prior to and after the plasma-surface interactions generated by the laser. The energy dispersive x-ray analyzer was used to study the removal of surface material after interaction with the plasma.

1. Laser

A neodymium-doped glass laser, with a wavelength of 1.06 μm, was the source of energy for producing a hot plasma over the target surface. The laser used was the two stage, KORAD K-1500 [62], operated in both the Q-switched and normal modes of operation. In the normal mode the pockels cell was removed from the oscillator cavity. A detailed description of the installation is given by Davis [11]. In Figure 11 a block diagram of the basic components of the system is shown.

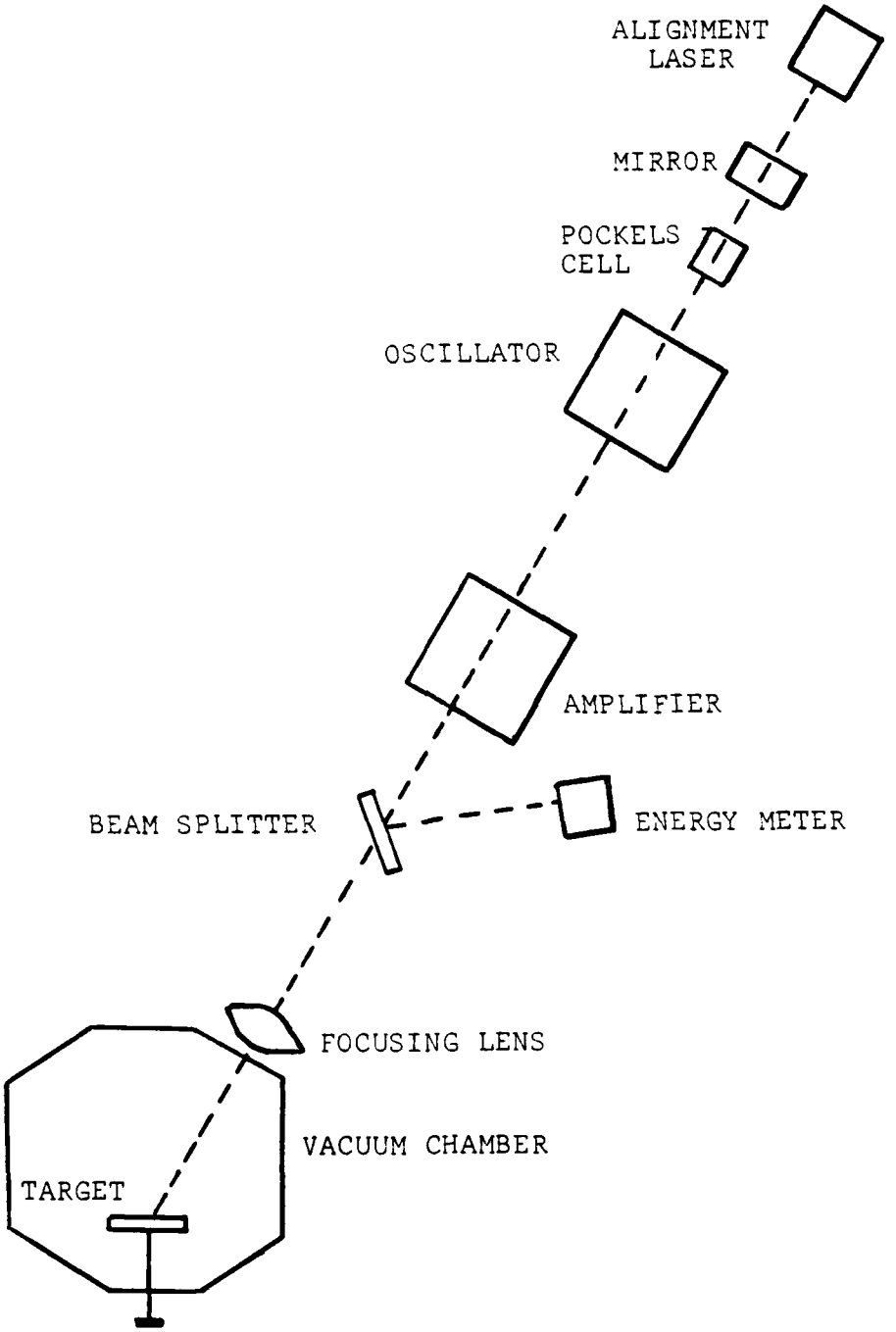

Figure 10. Laser and test chamber arrangement.

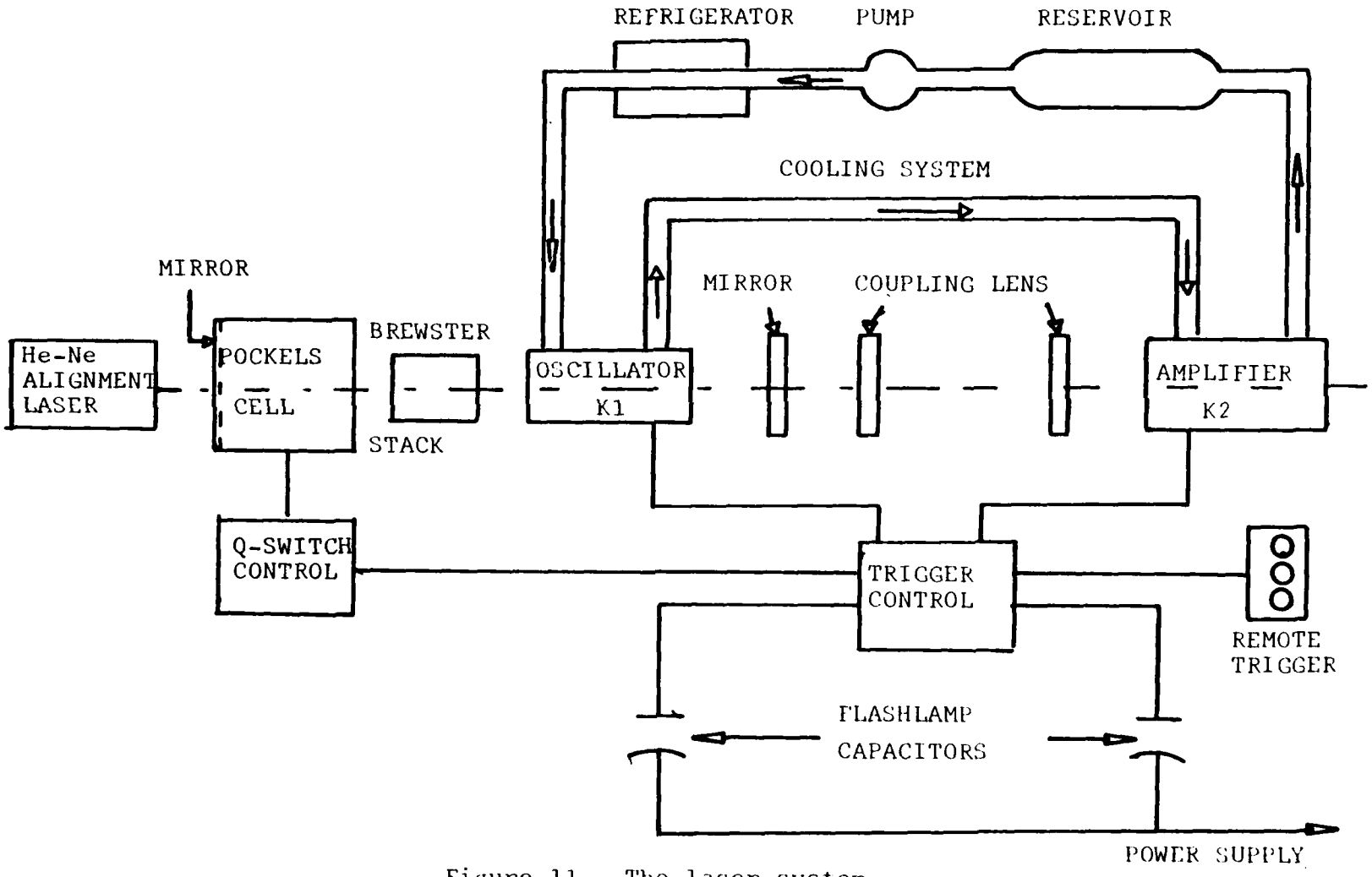

Figure 11. The laser system

The output energy of the laser is variable in the range of 0.2 - 15 J, by means of altering the voltages applied to the oscillator and amplifier flashlamps. For this experiment the laser was operated at an output level of about 15 J and reduction of energy at the target to about 3 - 5 J was accomplished by transmission filters placed in line with the laser radiation. This method was chosen because the laser sometimes failed to oscillate properly at lower voltage levels.

The laser total output energy was measured using a Laser Precision RK-3200 Series Pyroelectric Energy Meter. The meter was calibrated to an accuracy of about 20% [29].

2. Target Test Chamber

The target test chamber was a 6 inch cube of unbaked aluminum with an internal volume of 12.0 ± .04 liters. The vacuum system, composed of a mechanical forepump and an oil diffusion pump, provided a chamber pressure on the order of 10^{-6} Torr. The laser beam was aligned 30 degrees from normal to the target surface, in order to allow the use of probes directly in front of the target without interference from the laser beam.

3. Optical Microscope

A Bausch and Lomb Balplan stereoscopic light microscope was used to photograph and observe the target surfaces. This microscope was also used to determine the appropriate depth of craters after irradiation.

4. Scanning Electron Microscope

The Cambridge Stereoscan S4-10 scanning electron microscope was used to characterize the target surface before and after irradiation. A schematic showing the basic functional assembly of the microscope is shown in Figure 12 [53]. All images reported in this study were formed from secondary electrons.

B. PROCEDURES

The experimental procedure was separated into three stages. Target preparation was the first step. This included the specimen machining, coating with TiC, and mounting of the targets. Prior to the plasma-surface interaction process, the target surfaces were examined by light and scanning electron microscopes to establish surface smoothness and uniformity of coating. The second step, that of plasma-surface interaction, was then accomplished in the laser laboratory. The final step was the re-examination of the target surfaces by light and scanning electron microscopes to determine the effects of the TiC coating on the degree of unipolar arcing damage.

1. Target Preparation

a. Before Coating

All specimens were made of type 304 stainless steel. Targets were either machined in a disk shape or rolled foil of about 0.5 mm thickness was used. The disks were machined on a lathe to a diameter of 1/2 inch and a thickness of 1/8 inch.

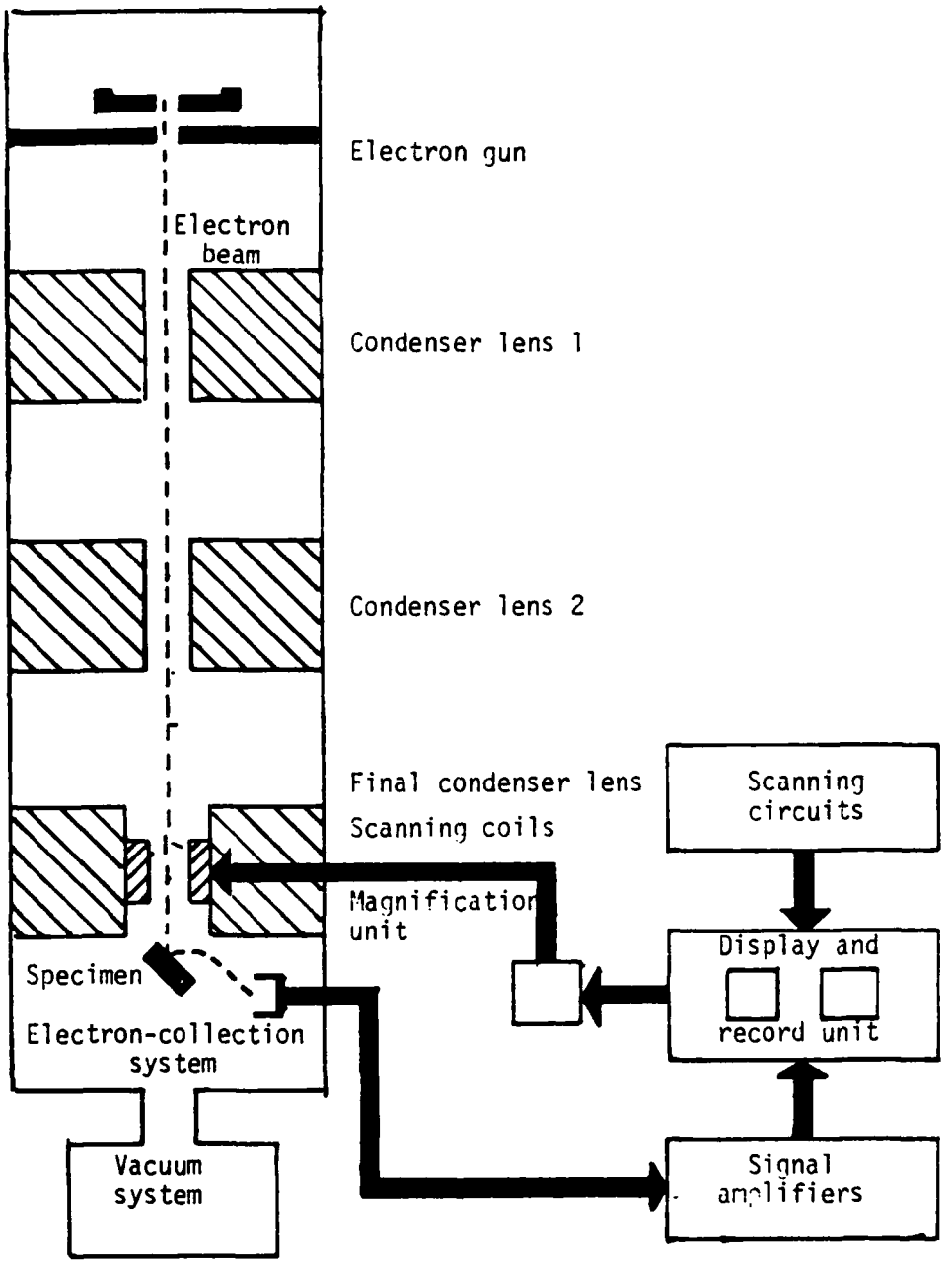

Figure 12. Scanning electron microscope.

b. TiC Deposition

The samples which received the TiC film were processed at the University of California at Los Angeles by the ARE deposition technique [7]. The substrate temperature was 550°C. A diagram of the deposition process is shown in Figure 9.

c. Target Surface Examination

After coating, each target was examined using both an optical and scanning electron microscope. Photographs were taken of surfaces in order to compare the appearance of the surface prior to the plasma-surface interaction with the damage observed after the interaction.

2. Plasma-Surface Interaction

Each specimen was cleaned with acetone and mounted in the test chamber. The laser was fired at energy levels of 3 - 6 J. and for a duration of about 1 millisecond for the normal mode or 25 - 30 nanosecond FWHM for the Q-switched mode. Breakdown was achieved establishing a hot, dense plasma of short duration over the specimen surface. The plasma established a sheath potential causing unipolar arcs and the resultant craters.

3. Surface Damage Investigation

Each specimen was inspected and photgraphed by optical and scanning electron microscope after laser irradiation. The surfaces were scanned for the presence of titanium using the PGT 1000 energy dispersive x-ray analyser. Depth of the

craters was determined using the optical microscope by focusing on the smooth target surface and the bottom of the crater. The difference in the focal distance established the crater depth.

IV. EXPERIMENTAL RESULTS

This study included three categories of targets subjected to plasma-surface interactions. The target used in experiment one was a stainless steel disk coated with a sputtered thin film of type 304 stainless steel. Experiment two was conducted on a .5 mm thick stainless steel foil, part of which was coated with TiC by the ARE process. Several targets were cut from the foil for mounting in the vacuum chamber. In experiment three the targets were unpolished type 304 stainless steel disks with half of one flat surface coated with TiC.

A. SPUTTERED STEEL COATING ON STAINLESS STEEL DISK

A laser produced plasma was used to deposit a film on a polished collector disk in the form of a half-circle [28]. Figure 13 shows the coating arrangement. The PGT 1000 x-ray analyzer was used to determine the composition of the coating on the disk [28].

The target was irradiated with the laser in the Q-switched mode, imparting an energy of 3J. Figure 14 shows the target after laser firing. The laser impact crater was about 0.75mm in diameter, surrounded by a plasma damaged surface area of about 3mm in diameter. The damaged surface closest to the laser impact crater is shown in Figure 15. This figure shows the molten appearance of this sample due to the longer duration

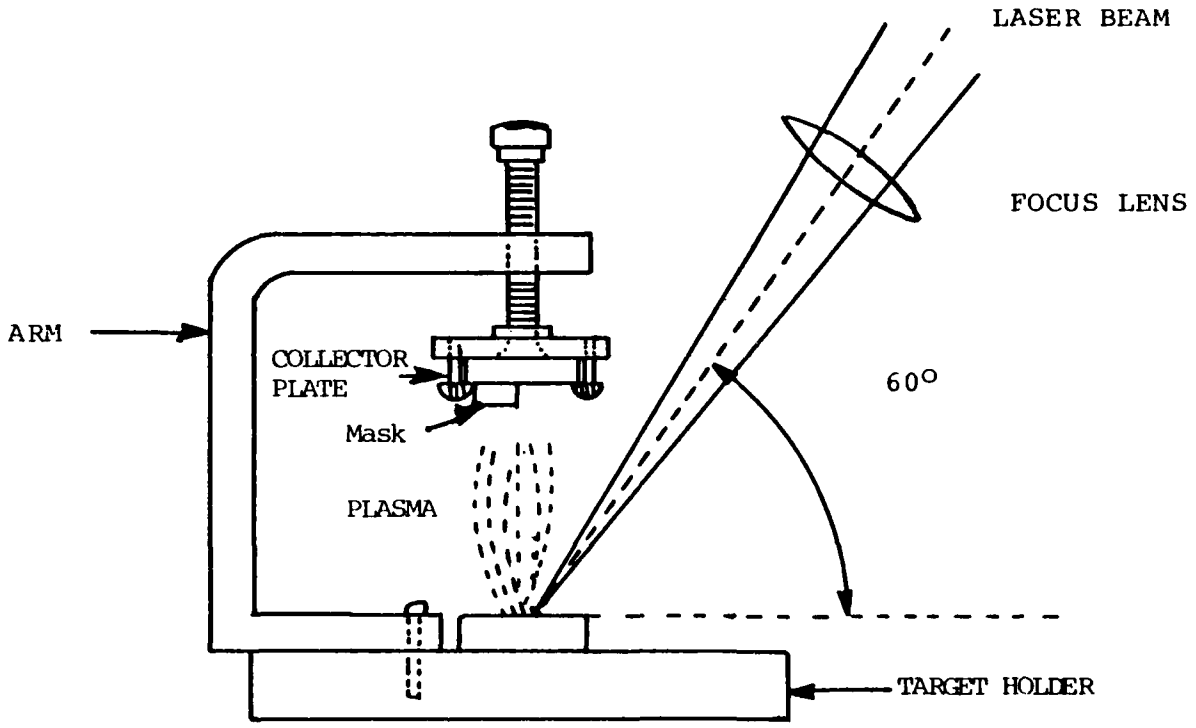

Figure 13. Target and collector arrangement

Figure 14. Stainless steel disk with stainless steel coating after laser irradiation

Figure 15. Overlapping "younger" and "older" craters. The laser impact area is beyond the right side of photo. 200 x magnification, by optical microscope

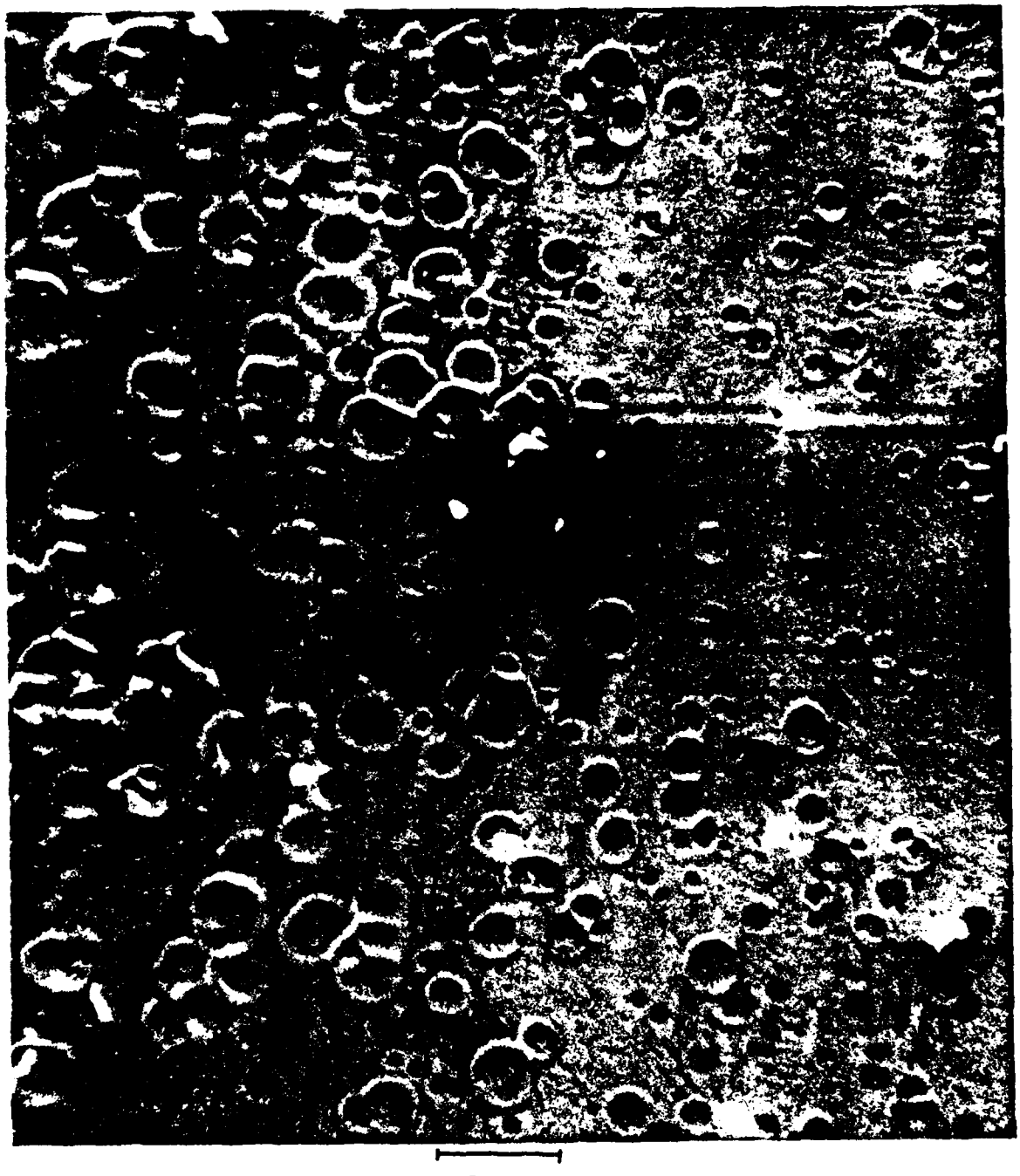

Figure 16. Crater formation at r ≈ 0.15 cm from laser focal spot which is located beyond left side. Crater density is of the order $3 \times 10^5/cm^2$. 200 x magnification, by SEM, photo enlarged.

of the plasma near the center of the impact crater. In Figure 16 the boundary between the area of multiple, longer duration arcs and the distinct, "younger" arcs is in the center of the photograph. The laser impact crater is to the left as shown. The area further removed from the impact crater, Figures 17 and 18, indicates that the unipolar arcing damage decreases in severity with increasing radial distance from the impact crater.

Although no external voltage was applied, about 20,000 unipolar arc craters were observable on the surface, which was exposed to the plasma for a few hundred nanoseconds. The oldest craters, resulting from arcs sustained for a longer time, have a diameter of 30 - 40 μm. These craters also exhibit significant metal flow resulting in a hemispherical shape and a pronounced rim. Other arcing craters, probably initiated toward the end of the plasma surface interaction period, have smaller diameters of about 10 μm and frequently exhibit a dark spot of approximately 1 μm in size. This dark spot is the cathode spot. Further analysis of a freshly formed cathode spot showed them to be nearly cylindrical in shape with a depth of 3 - 6 μm.

In this experiment it was observed that the sputtered stainless steel coating, applied at ambient temperature in a vacuum [28], exhibits poor adhesion to the substrate of identical composition. It was also determined that unipolar

Figure 17. Removal of Fe-Cr coating (darker areas) from polished stainless steel surface by plasma contact. 200 x magnification, by SEM, enlarged photo.

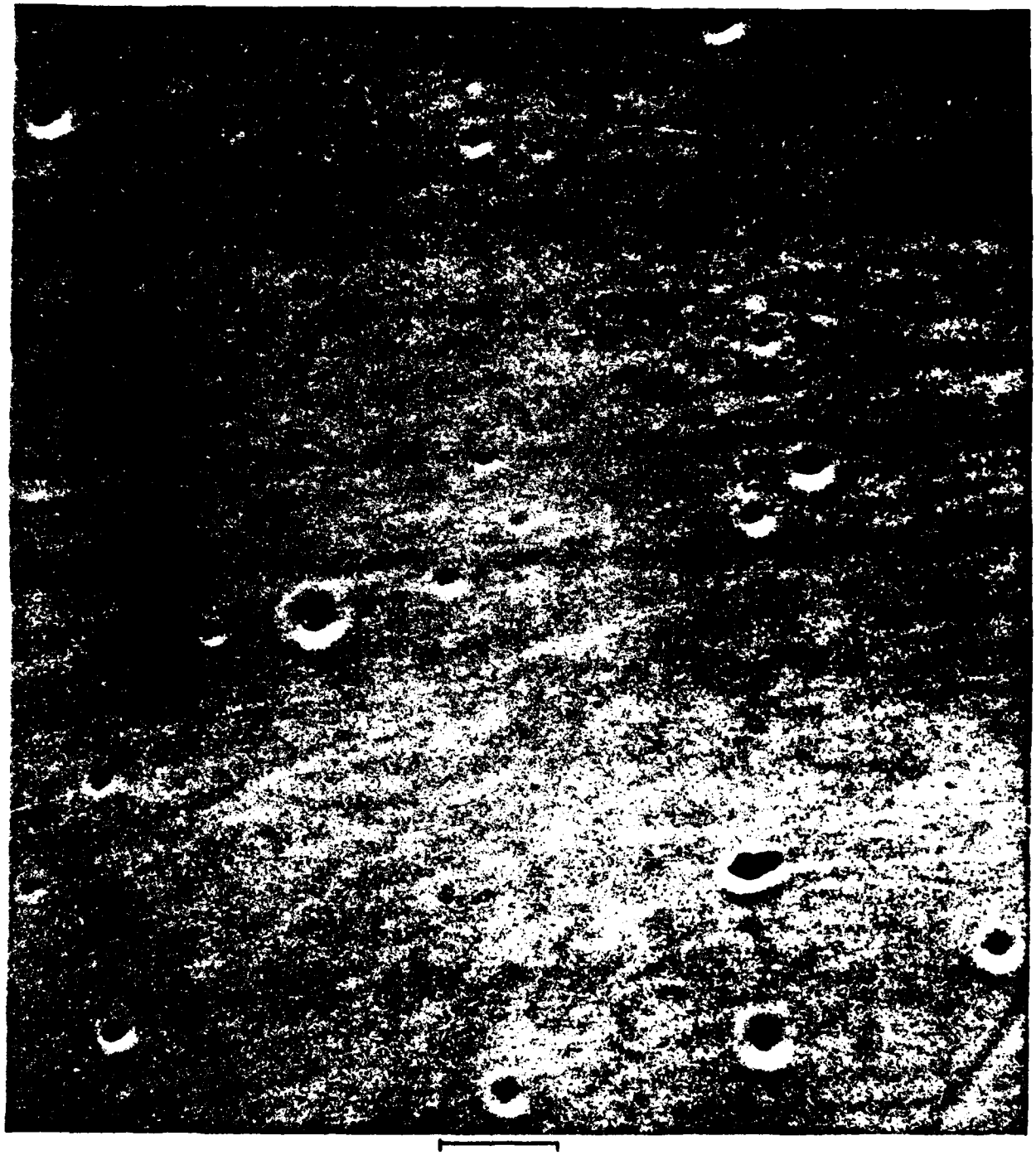

Figure 18. Onset of unipolar arc crater formation on highly polished stainless steel surface. 1000 x magnification, by SEM, enlarged photo.

arcs initiate from a cathode spot of 1 μm in diameter. This crater grows from the initial cylindrical cathode spot to a hemispherical crater with a diameter of 10 - 40 μm if the arc is sustained for sufficient duration to cause melting. A rim is formed due to the outward (radial) flow of molten metal caused by plasma pressure. Reflow after the arc ceases tends to cover the initial cathode spot and leave a hemispherical crater.

B. STAINLESS STEEL FOIL WITH TiC FILM

1. Reference Experiment Without TiC Film

The samples that were not coated with TiC showed evidence of significant unipolar arcing. The foil surface was irradiated in the rolled condition which left a relatively rough surface even where there was no plasma damage. In fact, where plasma damage is evidenced by the presence of craters, the plasma seems to have a smoothing effect on the immediate surface area. This effect has also been observed by Hantzsche [21].

In Figure 19 the plasma damage is shown on the left side. Craters 10 - 15 μm in diameter are distinguished by the molten rims and center cathode spots. The general smoothing effect is also observable in the area surrounding the craters. The plasma interacting with this sample was generated by a laser pulse of 4J in the normal mode.

Figures 20 and 21 show the damage resulting from a Q-switched laser pulse of 5J. As a result of the assymmetric

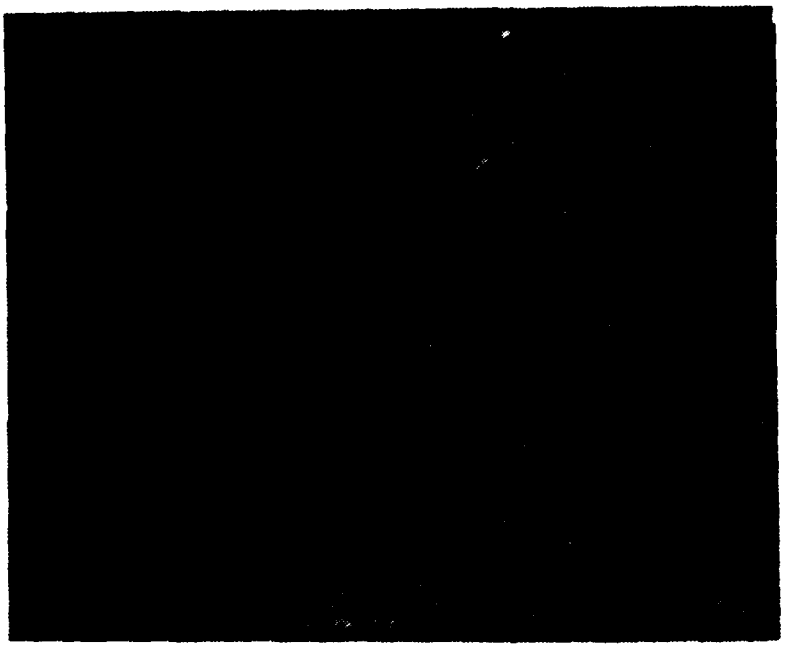

Figure 19. Cratering and surface smoothing effects on uncoated stainless steel foil, normal laser mode, 400X magnification by optical microscope.

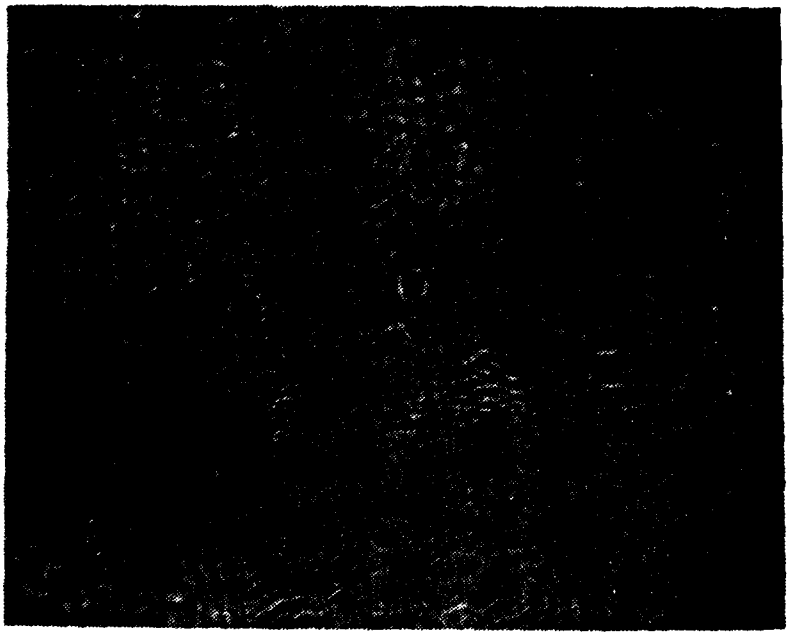

Figure 20. Craters adjacent to center damage region, Q-switched mode, 400X magnification, by optical microscope.

Figure 21. Arc tracks produced by plasma jet, laser impact area is toward the bottom: 400X magnification by optical microscope.

Figure 22. TiC coated foil surface, prior to laser irradiation, 400X magnification by optical microscope.

beam pattern of the laser during these firings the plasma flow was quite different from the circular pattern of experiment one. The resultant pressure gradients produced plasma jet effects evidenced by the arcing tracks shown in Figure 21. As shown by Figure 20, the plasma appeared to separate from the surface and "touch down" further out as seen by the gap between the overlapping craters near the impact crater, shown at the bottom left, and the isolated craters at the center of the photograph. In Figure 21 the impact crater is toward the bottom which shows the consistently decreasing size of craters with increasing radial distance, even when influenced by the "jetting" effect of the pressure gradients. The craters started about 0.1 mm from the overlapping center region, with a diameter of 15 - 18 μm and continued radially another 0.3 mm outward where crater diameters were 1 - 3 μm in diameter corresponding to the first stages of arc formation and arc damage.

2. Foil Coated with TiC by ARE Process

The samples coated with TiC displayed many unique effects. Unipolar arcing craters, as a manifestation of plasma-surface interaction, were not observed. Some craters were observed on the surface, but were apparently introduced during the ARE coating process due to substrate pits. Figure 22 shows the craters on the surface prior to laser irradiation, which are comparable in size and appearance to those observed after laser firings. Also apparent in Figure 22

is the replication of surface topography by the coating process, which is evident by comparing the general surface roughness with that of the uncoated foil in Figures 19, 20 and 21.

Since the observed damage effects on the coated samples were significantly altered by changing from the normal to Q-switched laser modes these cases were considered separately. The laser pulse energy for studies in the normal mode was 5 - 6 J with a pulse duration of about 1.0 ms. In the Q-switched mode, energies were comparable however the pulse duration was 25 - 30 nanoseconds.

a. Normal Pulse Damage Effects

The most notable observation was the absence of unipolar arcing craters. Although craters are observable in Figure 23, taken near the laser impact damage area, these craters are consistent with the size and appearance of those in the coating prior to irradiation. Also seen in Figure 23 is the chipping out of sections of the TiC coating and cracks at the boundaries of these chips. At the laser impact damage area the coating of TiC was virtually removed as shown in Figures 24 and 25, where the stainless steel substrate shows molten flow and splashing on top of the surrounding TiC film. Figure 25 is a PGT-1000 mapping of titanium over the same area which shows that the titanium concentration was substantially reduced in the molten area.

Figure 23. TiC coated foil near laser impact area, normal laser mode, 400X magnification by optical microscope.

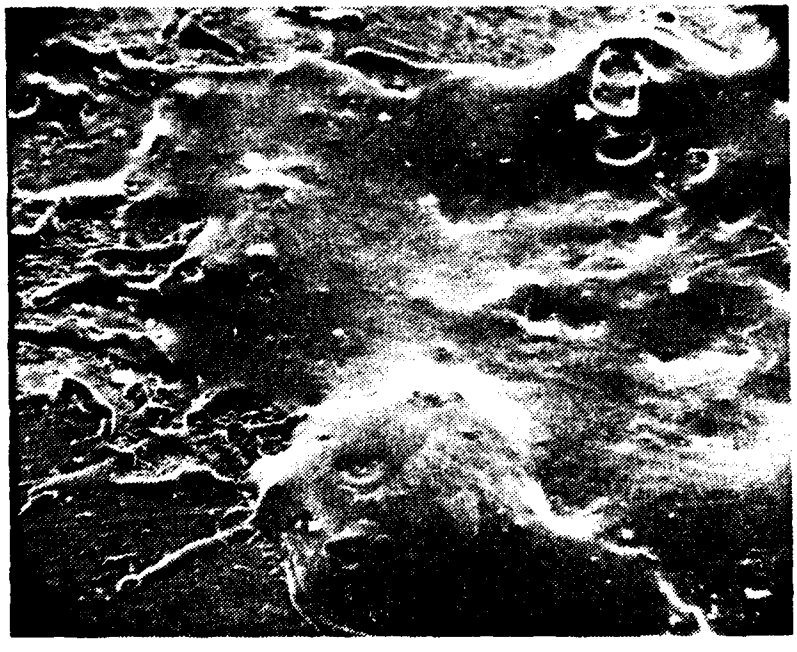

Figure 24. TiC coated foil laser impact damage area, normal laser mode, 100X magnification by SEM.

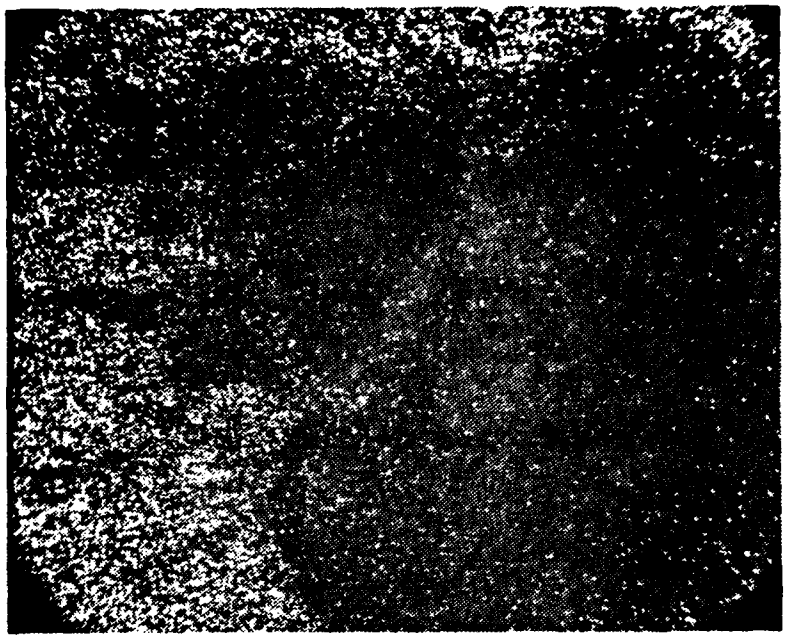

Figure 25. X-ray analyzer mapping of titanium over region shown in Figure 24.

Figure 26. Cracking of TiC coating at molten interface, normal laser mode, 400X magnification by optical microscope.

Figure 27. TiC "chip" floating on molten stainless steel, 400X magnification by optical microscope.

Figure 28. TiC coating near molten boundary of laser impact area, normal laser mode, 5000 x magnification by SEM.

An interesting effect, which occurred more noticeably with normal mode samples exposed to a laser pulse was cracking at the boundaries of molten stainless steel and solid TiC. Figures 26 and 27 show this effect, with Figure 27 showing a TiC chip floating on the top of a molten ridge of stainless steel. In Figure 28, taken at the boundary of the molten area, cracks are observed on a very small scale. Also observable in the lower right hand corner is the layered appearance of the TiC coating.

Due to the long pulse duration in the normal mode, it appears that the laser heating led to melting of the stainless steel substrate much sooner than the melting or breakdown of the TiC surface coating. As the laser pulse continued, the TiC cracked due to expansion of the stainless steel which allowed the TiC to be "blown away" by the remainder of the laser pulse. Evidence of this is shown in Figures 24 and 28 where the molten area is shown to have lower titanium concentration than the coating by PGT-1000 analysis.

The underlying TiC layers in Figure 28 show a sharp breaking line even at relatively high magnification.

b. Q-switched Pulse Damage Effects

In the Q-switched laser mode of plasma generation the TiC coated samples did not show the same evidence of unipolar arcing craters as stainless steel. The small craters observed as shown in Figure 29 were again similar in character to the craters resulting from the coating process. The

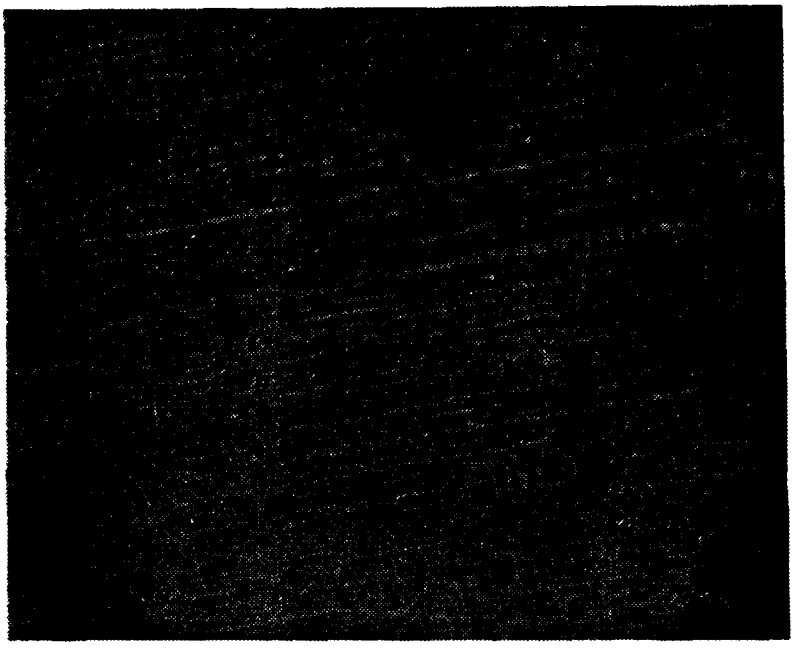

Figure 29. TiC surface near laser damage area, impact area is to the left bottom, Q-switched laser mode, 400X magnification by optical microscope.

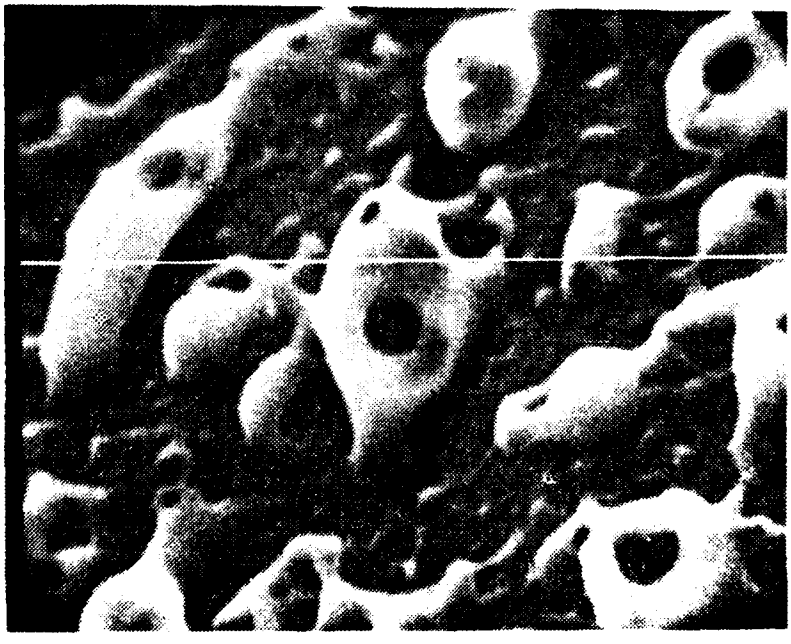

Figure 30. TiC coating after irradiation in laser impact area, 8000 x magnification by SEM.

larger dark areas are plasma damaged areas. The unique effect observed on the Q-switched mode samples was the fine, "honeycomb" appearance of plasma damaged areas and of the laser impact area. This is shown as dark areas in the bottom left hand corner of Figure 29 and is seen at higher magnification in Figures 30 and 31. This glassy surface effect was the only observable damage. The surface affected was of comparable area to the molten area of the uncoated samples in the Q-switched mode. Figure 32 shows a PGT-1000 mapping of the titanium density of the damaged area shown in Figure 30. A similar mapping for iron, chromium, and nickel showed that none of these were present on the surface.

The boundary between the damaged area and the coating surface is shown in Figure 33. The corresponding PGT-1000 mapping, shown in Figure 34, shows that the titanium concentration in the damaged area is the same as in the normal surface.

C. STAINLESS STEEL DISK WITH TiC FILM

1. Reference Experiment Without TiC Film

The disk targets used for this portion of the study were half-coated with TiC by the ARE process. The disk surface was coated while in machined condition. Figure 35 shows the surface conditions prior to coating. These conditions also prevailed during laser irradiation of the uncoated portion of the targets. In Figures 36 and 37 the overlapping craters near the laser impact area are shown. As with the

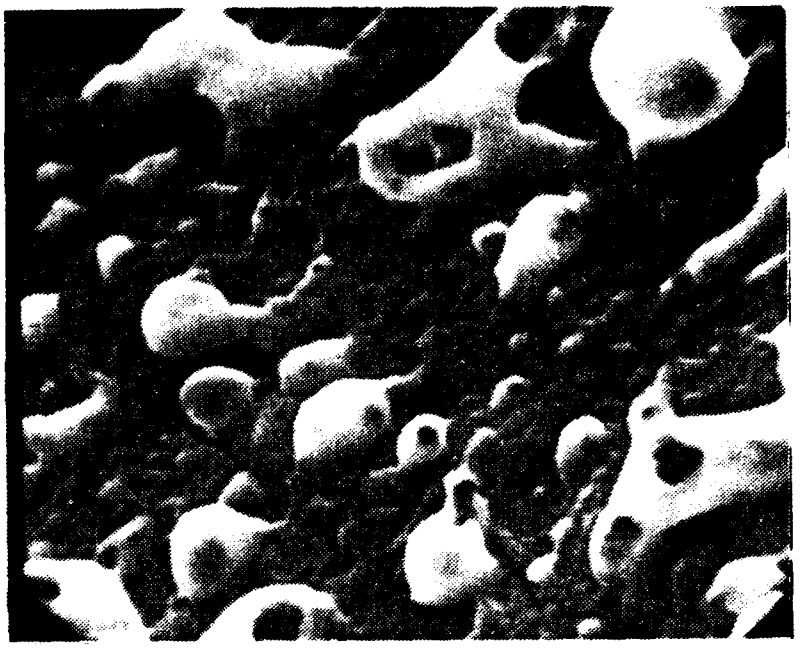

Figure 31. TiC coating at laser impact area showing cracking, Q-switched laser mode, 8000 x magnification by SEM.

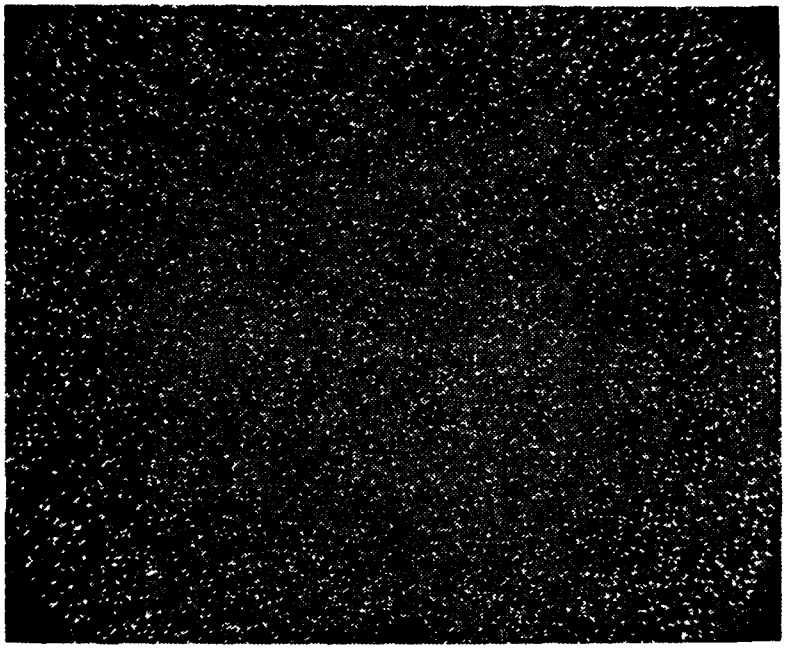

Figure 32. X-ray analyzer mapping of titanium on region shown in Figure 30.

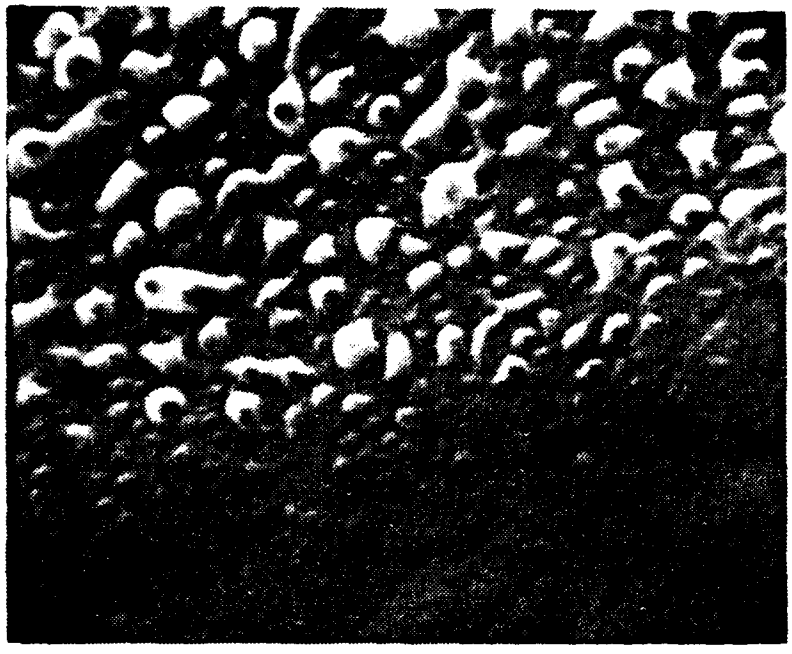

Figure 33. Boundary of laser damage area on TiC coating, Q-switched laser mode, 8000 x magnification by SEM.

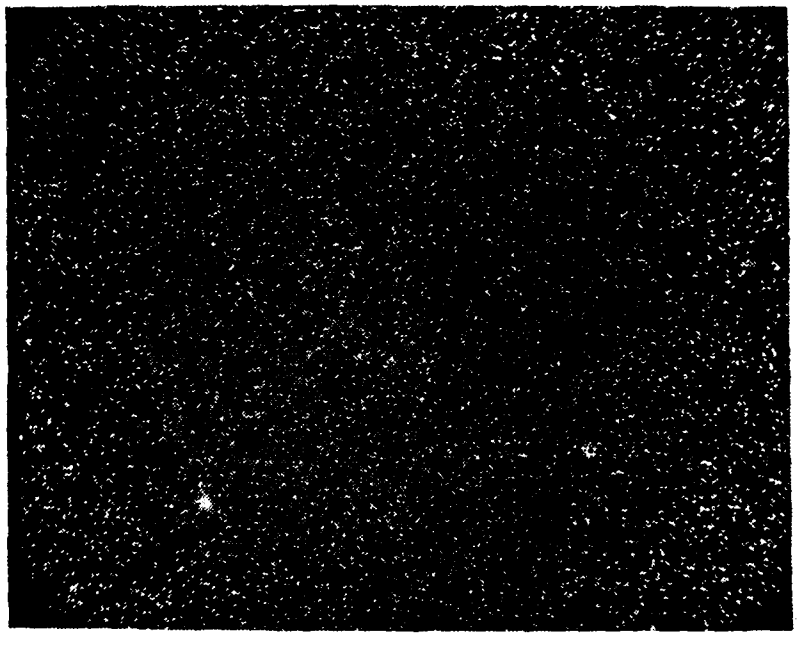

Figure 34. X-ray analyzer mapping of surface shown in Figure 33.

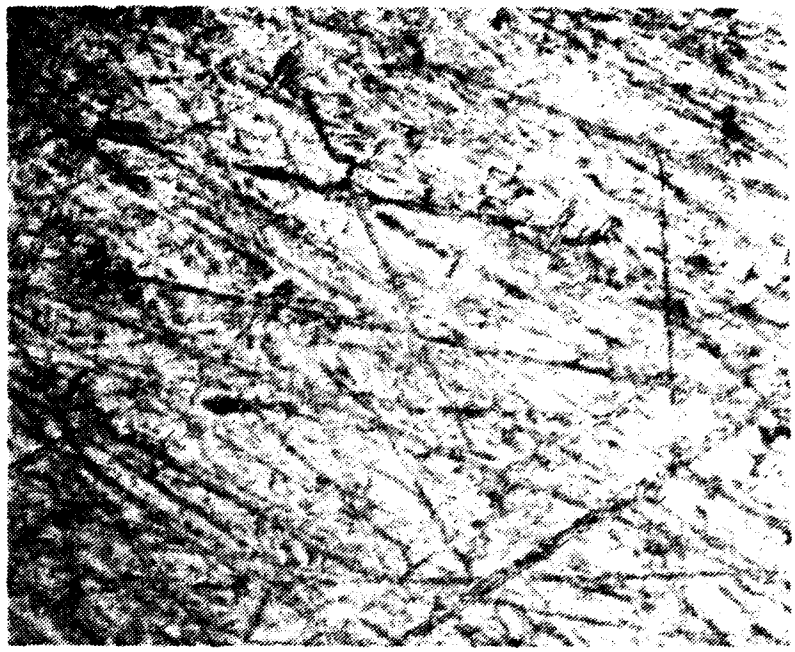

Figure 35. Stainless steel disk machined surface without TiC coating, 400X magnification by optical microscope.

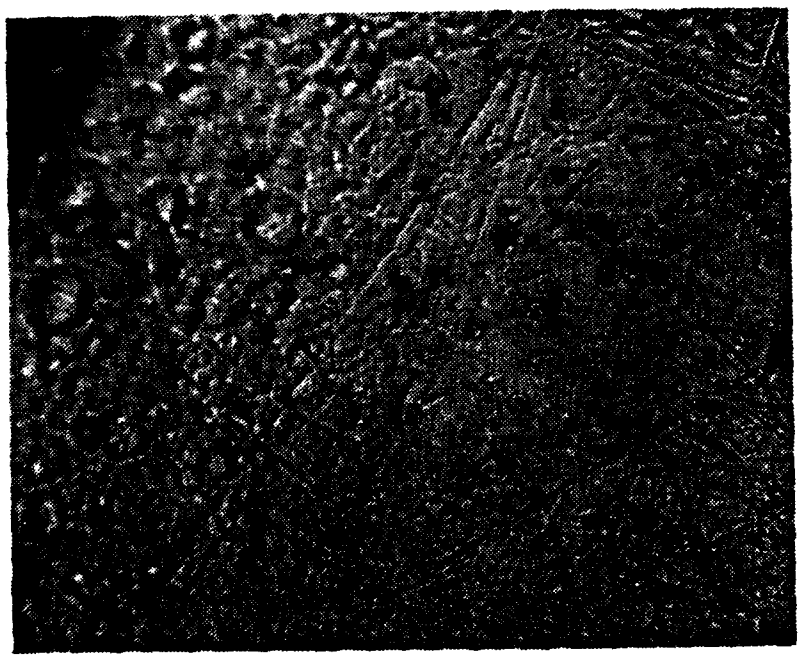

Figure 36. Molten damage area and individual craters on stainless steel disk, Q-switched laser mode, 400X magnification by optical microscope.

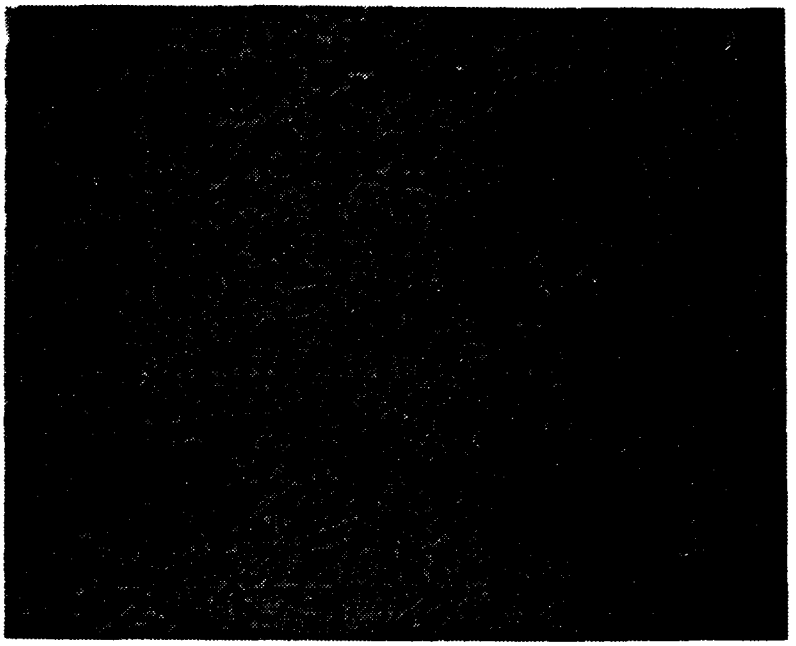

Figure 37. Boundary of molten, overlapping crater area, stainless steel surface, Q-switched laser mode, 400X magnification by optical microscope.

Figure 38. TiC coating on stainless steel disk prior to laser irradiation, 400X magnification by optical microscope.

uncoated foil samples, the craters show the molten appearance with a clearly distinguishable rim. Figure 36 shows several individual craters just outside the molten area.

The sample seen in Figures 36 and 37 was irradiated with a 5J laser pulse with a pulse duration of 25 - 30 nanoseconds. The surface smoothing effect observed in the foil samples is also evident in Figure 36.

2. Disk Samples Coated With TiC by ARE Process

The disk samples coated by ARE had a rough, pitted surface, prior to irradiation due to replication of the substrate as seen in Figure 35. Figure 38 shows that the smaller scratches in the surface are filled in by the deposition process whereas the deeper scratches tend to develop circular pits. Figure 39 shows one of these pits at higher magnification. The upper coating layer is about 3 μm thick.

In spite of the roughness of these surfaces it was clear that arcing craters were not observable in the coating. Figure 40 shows the surface of the coated sample about 0.1 mm from the laser impact damage (dark area on left hand side). The larger spheres are deposits on top of the surface which were "blown out" from the laser impact area. In comparison to the melting and smoothing of the stainless steel surface in Figure 37, no such effect is observable on the TiC coated sample, indicating no melting. The melting temperature of stainless steel is approximately 1526 °C while that of titanium carbide is approximately 3430 °C. As with the TiC coated

Figure 39. Surface pitting in TiC coating, prior to laser irradiation, 5000 x magnification by SEM.

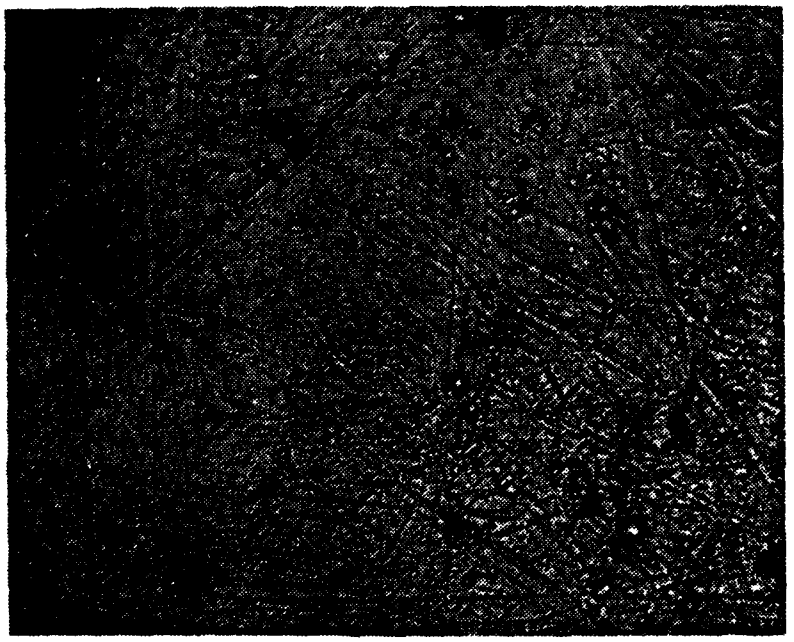

Figure 40. TiC coating near center impact area, Q-switched laser mode, 400X magnification by optical microscope.

foil samples the disk samples displayed the honeycomb appearance in the laser impact region as shown in Figures 30 and 31.

In the normal mode of laser irradiation cracking of the TiC coating was evident with the disk samples as with foil. Figure 41 shows this cracking at the boundary of the molten center damage area.

Figure 41. Cracking in TiC coating at molten boundary of center laser impact area, normal laser mode, 400X magnification by optical microscope.

V. DISCUSSION

A. THE PROCEDURE

Unipolar arcing was studied using a focused, pulsed laser to generate a plasma from the target materials. The laser was used both in the Q-switched and normal pulse modes. This technique provided a hot, dense plasma which was rapidly (25 - 50 ns) generated at a specific point on the target. The target was subjected to a plasma density gradient as the plasma expanded. Using a hemispherical expansion model, the plasma which was 100 eV, 10^{21} cm^{-3} initially decreased in density as it expanded over the surface radially. The innermost surface was exposed to this dense plasma while the outer surface was subjected a lower density plasma. No arc craters were found on the TiC coated samples at any location.

B. CONDITIONS THAT PROMOTE UNIPOLAR ARCING

The minimum requirement for the onset of unipolar arcing is that the sheath potential is comparable to the ionization energy. Local micro-inhomogeneities exist either in the form of surface projections and whiskers or in the form of dielectric spots and inclusions. Apparently all metals, polished or not, have micro-whiskers which can be erected in the presence of the plasma [39]. The dielectrics are metalurgical impurities or surface contamination such as oil and absorbed films of water and gases.

The whiskers act much as an antenna or lighting rod and establish strong local fields which promote arcing. They provide a near plasma point which can be heated easily by ion bombardment and act as a source of particles which enter the plasma, become ionized, and increase the local plasma density. The oils/gases are also heated by the plasma contact, desorb from the surface and serve in the same fashion as the whiskers to increase the local plasma density.

C. INITIATION OF UNIPOLAR ARCING

From the work of Langmuir and of Bohm, it is known that when a plasma and electrically isolated metal are in equilibrium, a floating sheath potential (U_f) is established such that the ion and electron leakage rates from the plasma to the wall are equal. The wall, at the floating potential, repels all but the fastest electrons in the Maxwellian distribution, and the net current is zero. If the electron temperature is sufficiently high, the floating potential (U_f) will exceed the potential required to initiate and sustain an arc.

The heat transfer rate from surface inhomogeneities is lower than the surrounding areas due to local geometry or material characteristics. This increased electric field strength due to inhomogeneities, increases the ion flux to these spots. Increased ion bombardment and recombination rates lead to increased surface temperature. This increased temperature leads to desorption and vaporization of neutrals

from the surface. Neutrals are emitted with thermal velocity corresponding to the surface temperature.

Not all such conditions lead to establishment of an arc crater however. If heating is sufficiently rapid, whiskers may be explosively removed from the surface; the local field is reduced and U_c returns to its initial value. The arc stops before crater formation occurs. This explains the "conditioning" of materials observed in other studies [36].

If the local plasma density is sufficient an arc is established which results in the formation of a visible crater. Figure 2 illustrates the fields and currents established in the area of a cathode spot.

D. CRATER FORMATION

A crater begins to form as material is removed from the surface. The center crater (cathode spot) is approximately 1 μm in diameter. The arc current produces a significant magnetic field. Based on an arc current of 10 amperes for a 1 μm diameter conductor, the magnetic field is 10^4 Gauss. This magnetic field does not have sufficient time to permeate the metal wall of the forming crater, and forces the plasma to exit in a narrow jet. The magnetic field also prevents particle interactions with the wall and results in a nearly cylindrical cathode spot crater. This crater was observed in all experiments and ranged in depth from 3 - 6 μm.

In the case when the arc duration is long, the magnetic field does permeate the crater wall toward the surface and

the particle interactions then heat the crater wall to a molten state in that area. The plasma jet pressure, pressing outward radially, causes molten metal to form a characteristic rim about the crater. Flow and reflow of molten metal cause the crater to take on a hemispherical shape (Figures 42, 43).

Figure 44 shows the various stages of arc crater formations.

E. ARC CESSATION

The density above the cathode spot is increased as new material from the crater enters the plasma. The arc continues until this influx of material is sufficient to cool the plasma electrons locally to the point where the arc can no longer be sustained. The density gradient within the plasma decreases due to diffusion. Due to these factors the plasma potential decreases to a value below that required to sustain an arc and the arc stops. The net current flow to the wall is zero and the floating potential returns to the original value. Using Equation 14 it can be seen that a decreasing temperature and a decreasing pressure gradient reduce the plasma potential hump. When it is reduced near the cathode spot to a level below that required to sustain the arc, the arc ceases.

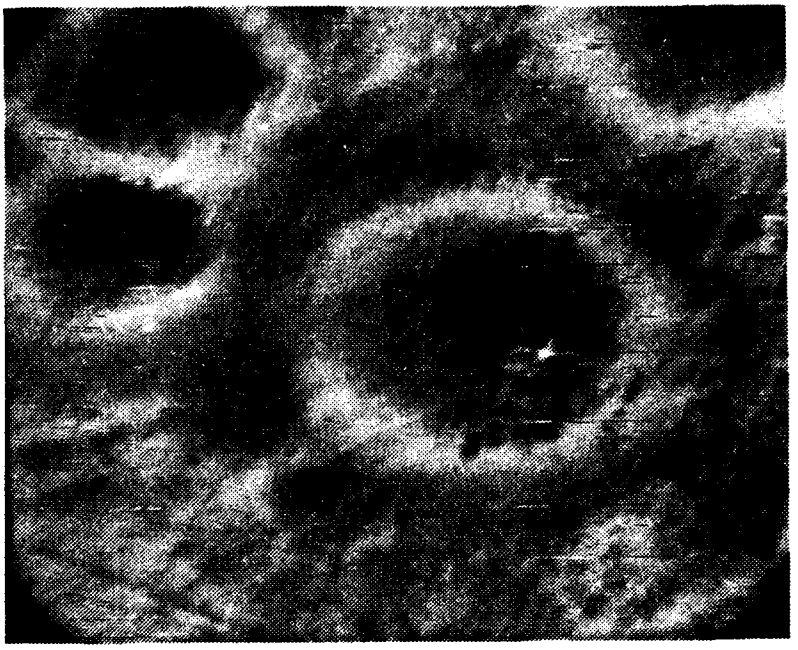

Figure 42. Arc crater in stainless steel, Q-switched laser mode, 5000 x magnification by SEM.

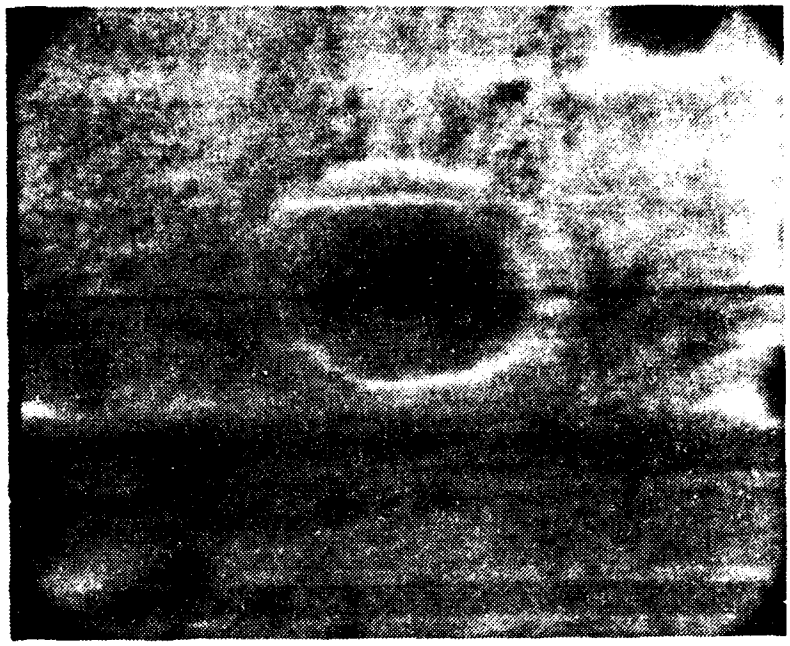

Figure 43. Arc crater in stainless steel showing cathode spot and well developed rim, 5000 x magnification by SEM

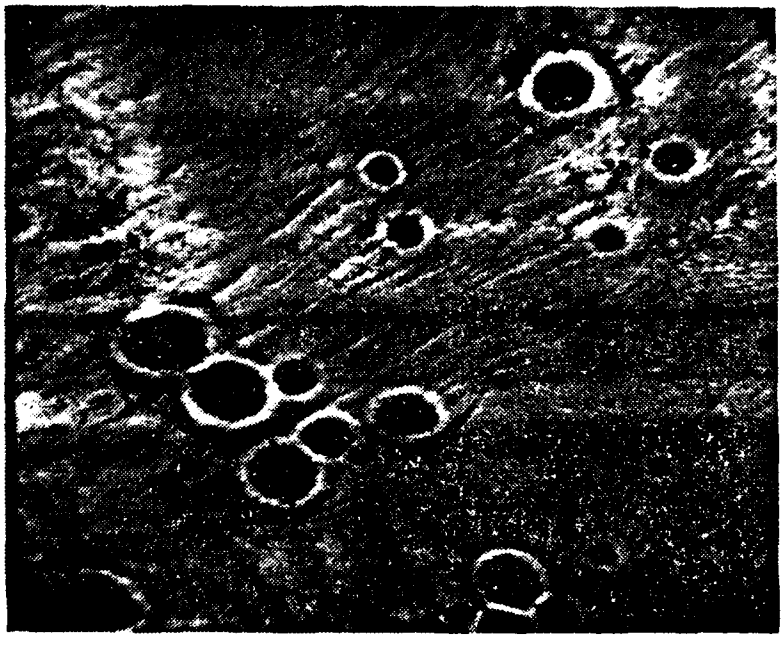

Figure 44. Stainless steel surface showing several craters at various development stages, 1000 x magnification by SEM.

VI. CONCLUSIONS

The study undertaken by this thesis had a dual thrust. The phenomenon of unipolar arcing was examined theoretically and experimentally resulting in the expanded model. Simultaneously the Activated Reactive Evaporation (ARE) deposition of TiC was experimentally investigated as a means of controlling or preventing unipolar arcing.

Although the most effective environment for unipolar arc initiation was generated with the laser in the Q-switched mode, other significant information was obtained as a result of normal mode laser irradiation. In the longer pulse, normal mode, the substrate was heated to the melting point prior to the coating. This was evidenced by the composition of the molten areas in Figure 24 and the cracks evident in Figures 26 and 27. Clearly this indicates that any such combination of materials for coating and substrate must be well matched in thermal expansion characteristics; and must be maintained at temperatures that are in general somewhat less than the temperature of the lower of the two melting points.

With the higher laser intensities generated during the Q-switched mode, the plasma conditions consistently produced unipolar arcing on the stainless steel surfaces. In contrast, no unipolar arc craters were observed on the surfaces coated with TiC when irradiated in either laser mode. In the normal

mode the cracking mentioned previously was certainly not a plasma effect, while in the Q-switched mode the damage appeared to be limited to the upper layer of the TiC film as shown in Figures 30 and 32. The coating apparently suffered breakdown on the surface and produced the plasma which interacted with the surface immediately adjacent to the laser impact area, causing vaporization and rapid resolidification at ambient temperature. While the surface area damaged by the laser was virtually equal to the area damaged on equivalent stainless steel samples; it is remarkable that a PGT 1000 analysis showed a homogeneous titanium distribution of the 5 μm coating of TiC throughout the damaged area, despite a laser intensity on target of 10^9 watts/cm^2.

Recognizing that there are many diverse considerations involved in the selection of wall materials for magnetically confined fusion devices, it appears that coatings of the type tested in this study could be the solution to the unipolar arcing problem.

BIBLIOGRAPHY

1. Ali-Khan, I., Dietz, K.J., Waelbroeck, F., and Wienhold, P., "Plasma Cooling by Metal Snow II. Discussion of Experimental Evidence," Journal of Nuclear Materials, v. 74, p. 138-143, June 1978.

2. Bausch and Lomb, Dynazoom Bench Metallograph Instructions, Second Edition. Second Printing, Rochester, New York.

3. Behrisch, R., Materials Problems in Energy Productions, Preprint, Academic Press, 1976.

4. Behrisch, R., "Surface Erosion from Plasma Materials Interaction," Journal of Nuclear Materials, v. 85-86, p. 1047-1061, 1979.

5. Bodhansky, J., Roth, J., and Brossa, F., "Formation of Various Coatings and Their Behavior Under Particle Bombardment," Journal of Nuclear Materials, v. 85-86, p. 1145-1150, 1979.

6. Buehler LTD, Instructions for the Operation and Maintenance of No. 67-1509 and 67-01510 AB Vibromet Polishers, Evanston, Illinois.

7. Bunshah, R.F., "Physical Vapor Deposition of Metals, Alloys, and Ceramics," paper presented at Material Science Symposium, Detroit, Michigan, October 1974.

8. Bunshah, R.F., Nimmagadda, R., and Dunford, W., "Structure and Properties of Refractory Compounds Deposited by Electron Beam Evaporation," paper presented at International Conference on Metallurgical Coatings, San Francisco, California, 3-7 April 1978.

9. Chen, F.F., Introduction to Plasma Physics, Plenum Press, 1974.

10. Daalder, J.E., "Erosion and the Origin of Charged and Neutral Species in Vacuum Arcs," Journal of Physics D, Applied Physics, v. 8, p. 1647-1659, August 1975.

11. Davis, L.J., Self-generated Magnetic Field Produced by Laser Bombardment of a Solid Target, M.S. Thesis, Naval Postgraduate School, Monterey, California, 1971.

12. Davis, W.D., and Miller, H.C., "Analysis of the Electrode Products Emitted by DC Arcs in a Vacuum Ambient," Journal of Applied Physics, v. 40, no. 5, p. 2212-2221, April 1969.

13. DeMaayer, P.J.P. and MacKensie, J.D., "The Electrical Properties of Thin Films of TiNx and TiCx," z. Naturforsch, v. 30, p. 1661-1666, October, 1975.

14. Drouet, M.G., "Plasma Expansion and Ion Flux from the Cathode Spot in a Vacuum Arc," paper presented IEEE International Conference on Plasma Science, Montreal, Canada, 4-6 June 1979.

15. Engel, A., Ionized Gasses, Claredon Press, 1955.

16. Furth, D.H., "Progress Toward a Tokamak Fusion Reactor," Scientific American, p. 51-61, August 1979.

17. Glancy, M.T. and Rose, M.F., "Surface Aging in High Repetition Rate Spark Switches with Aluminum and Brass Electrodes," paper presented at 2nd IEEE International Pulsed Power Conference, Lubbock, Texas, 12-14 June 1979.

18. Glasstone, S. and Lovberg, R.H., Controlled Thermonuclear Reactions, D. Van Nostrand, 1960.

19. Culham Laboratory (UKAE) Report CLM-R 167, Arcing and Surface Damage in DITE by D.H.J. Goodall and G.M. McCracken, November 1977.

20. Greene, J.E., Woodhouse, J., and Pestes, M., "A Technique for Detecting Critical Loads in the Scratch Test for Thin Film Adhesion," Review of Scientific Instrumentation, v. 45, no. 6, p. 747-749, June 1974.

21. Hantzsche, E., Juttner, B., Rohrbeck, W., and Wolff, H., "Erosion of Metal Cathodes by Arcs and Breakdowns in Vacuum," Journal of Physics D, Journal of Applied Physics, v. 9, p. 1771-1781, April 1976.

22. Culham Laboratory (UKAE) Report CLM-P 535, The Effect of Secondary Electron Emission on a Plasma Sheath, by P.J. Harbour, May 1978.

23. Culham Laboratory (UKAE) Report CLM P 528, The Influence of Electron Emission at Divertor Target of a Tokamak Fusion Reactor, by P.J. Harbour and Harrison, M.F.A., April 1978.

24. Harbour, P.J. and Harrison, M.F.A., "The Influence of Electron Emission at the Divertor Target of a Tokamak Fusion Reactor," Journal of Nuclear Materials, v. 76-77, p. 513-517, September-October 1978.

25. Horvath, Von E., Happel, O., und Perry, , A.J., "Verschleib feste Beschichtung von Stahl mit dem CVD-Verfahren," Metall ober flaeche, v. 32, no. 8, p. 343-347, 1978.

26. Horvath, E. and Perry, A.J., "The Wear-Resistant Coating of Steel by Chemical Vapour Deposition," Wear, v. 48, p. 217-224, June 1978.

27. Hugill, J., "An Arc-resistant Target for the Divertor of a Fusion Reactor," Journal of Nuclear Materials, v. 87, no. 23, p. 353-355, December 1979.

28. Hwang, Z.W., Laser Induced Evaporation from Stainless Steel Surfaces, Master's Thesis, Naval Postgraduate School, Monterey, California, December 1978.

29. Johnson, C.B., Induced Evaporation of Metal from an Aluminum Surface by a Normal Pulse Neodymium Laser, Master's Thesis, Naval Postgraduate School, Monterey, California, 1979.

30. Karlau, J., Martin, C., Muller, K.G., and Tuczek, H., "Diagnostic of Unipolar Arcs," Journal of Nuclear Materials, v. 76-77, p. 504-507, September-October 1978.

31. Kimblin, C.W., "Erosion and Ionization in the Cathode Spot Regions of Vacuum Arcs," Journal of Applied Physics, v. 44, no. 7, p. 3074-3081, July 1973.

32. Kodama, M., Shabaik, A.H., and Bunshah, R.F., "Machining Evaluation of Cemented Carbide Tools Coated with HfN and TiC by the Activated Reactive Evaporation Process," paper presented at International Conference on Metallurgical Coatings, San Francisco, California, 3-7 April 1978.

33. Malinowski, M.E., "Clean and Contaminated TiD_2 Films: Fabrication and Auger Spectra," Journal of Vacuum Science and Technology, v. 15, no. 1, p. 39-43, January-February 1978.

34. Malinows-i, M.E., "Deuteriding of Thin Titanium Films: The Effect of Carbon Monoxide Surface Contamination," Journal of Nuclear Materials (Holland), v. 63, p. 386-391, 1976.

35. May, V.M. and Bertram, C.H., "Beitrag zur Frage der Initialvor-gange bei der Chemischen Abscheidung von TiC aus der Gasphase auf Eisenwerkstoffe," Neue Huette, v. 17, no. 6, p. 328-333, 1972.

36. Culham Laboratory (UKAE) Report CLM-P 573, "Plasma-Surface Interactions in Tokamaks," by G.M. McCracken and P.E. Stott, 1979.

37. Metals Handbook, 8th ed., v. 2, American Society for Metals, 1964.

38. Miley, G.H., "Plasma Surface Arcing in Fusion Devices," paper presented at International Conference on Plasma Science, Montreal, Canada, 4-6 June 1979.

39. Miley, G.H., "Surface Effects Related to Voltage Breakdown in CTR Devices," Journal of Nuclear Materials, v. 63, p. 331-336, December 1976.

40. Mioduszewski, P., Clausing, R.E., and Heatherly, L., "Wall Erosion by Plasma Induced Arcing," paper presented IEEE International Conference on Plasma Science, Montreal, Canada, 4-6 June 1979.

41. Mitsunori, K. and Yoshihiko, D., "TiN and TiC Coating on Cemented Carbides by Ion Plating," paper presented at International Conference on Metallurgical Coatings, San Francisco, California, 3-7 April 1978.

42. Nakamura, K., Shinoki, F., and Itol, A., "Preparation of TiC Film by R.F. Reactive Sputtering," Japanese Institute of Metals Journal, v. 33, no. 10, p. 913-919, October 1974.

43. Nedospasov, A.V. and Petrov, V.G., "Model of the Unipolar Arc on a Tokamak Wall," Journal of Nuclear Materials, v. 76-77, p. 490-491, September-October 1978.

44. Nozawa, Y., Inagawa, K., Komiya, S., and Nakamura, K., "Application of Titanium Carbide Thick Films Deposited by the LPPD Process to High Speed Steel Tools," paper presented at International Conference on Solid Surfaces, 3rd, v. 2, p. 1745-1748, Vienna, Austria, 12-16 September 1977.

45. Nurnberg, A.W., Bauder, U.H., and Behrisch, R., "Cathode Erosion in Vacuum Arcs and Unipolar Arcs," paper presented at 4th International Conference on Plasma Surface Interactions in Controlled Fusion Devices, Garmisch-Partenkirchen, Federal Republic of Germany, 21-25 April 1980.

46. Ohmae, N., Tsukizoe, T., and Nakai, T., "Ion-plated Thin Films for Anti-wear Applications," Journal of Lubrication Technology, v. 100, p. 129-135, January 1978.

47. Operators Manual, The PGT-1000 Disc System, Software Version 70, August 1976.

48. Oren, L., Schwirzke, F., and Taylor, R.J., Physical Review Letters, v. 40, p. 1181, April-June 1978.

49. Oren, L., Taylor, R.J., and Schwirzke, F., "Phenomenology of Metal Influx in Macrotor," Journal of Nuclear Materials, v. 76-77, p. 412-417, September-October 1978.

50. Petr, R., Barrett, D., and Burkes, T.R., "Spark Gap Erosion Results," paper presented at 2nd IEEE International Pulsed Power Conference, Lubbock, Texas, 12-14 June 1979.

51. Robson, A.E. and Thoneman, P.C., "An Arc Maintained on an Isolated Metal Plate Exposed to a Plasma," Physical Society of London Proceedings, v. 73, p. 508-512, January-June 1959.

52. Rossikhin, V.S. and Vovk, V.I., "Some Spectroscopic Properties of a Unipolar Arc Discharge in an Argon Atmosphere," Journal of Applied Spectroscopy (USSR), v. 19, no. 1, p. 831-834, July 1973.

53. S4-10 Stereo Scanning Electron Microscope Manual, TL 1116-OM-96118-002, Cambridge Scientific Instruments Limited.

54. Schwirzke, F., Active Control of Plasma Wall Interactions, private research notes, April 1980.

55. Schwirzke, F. and Taylor, R.J., "Arcing, an Experimental Investigation of Plasma Surface Interaction," Bulletin American Physical Society, v. 24, p. 971, November 1979.

56. Schwirzke, F. and Taylor, R.J., "Surface Damage by Sheath Effects and Unipolar Arcs," paper presented 4th International Conference on Plasma Surface Interactions in Controlled Fusion Devices," Garmisch-Partenkirchen, Federal Republic of Germany, 21-25 April 1980.

57. Sharma, N.K. and Williams, W.S., "An Auger Analysis of Substrate-Layer Interactions in the Chemical Vapor Deposition and Activated Reactive Evaporation of TiC," paper presented at the International Conference on Metallurgical Coatings, San Francisco, California, 3-7 April 1978.

58. Sharma, N.K. and Williams, W.S., "Interface Between Chemically Vapor Deposited Titanium Carbide and Cemented Carbide Substrate," Journal of American Ceramic Society, v. 62, no. 3-4, p. 193-198, March-April 1979.

59. Sharma, N.K., Williams, W.S., and Gottschall, R.J., "Investigation of the Interlayers between Cemented Carbides and Titanium Carbide Coatings Obtained by Chemical Vapor Deposition," paper presented at International Conference on Metallurgical Coatings, San Francisco, California, 28 March - 1 April 1977.

60. Oak Ridge National Laboratory Report 5222, Product Form Characterization of Type 304 Stainless Steel (HT 9T2796), by R.W. Swindeman, W.J. McAfee, V.K. Sikka, H.E. McCoy, Jr., and R.D. Waddell, Jr., February 1977.

61. Tien, J.K., Panayoyou, N.F., Stevenson, R.D., and Gross, R.A., "Unipolar Arc Damage of Materials in a Hot, Dense Deuterium Plasma," Journal of Nuclear Materials, v. 76-77, p. 481-488, September-October 1978.

62. Union Carbide Electronics, KORAD Laser Systems Instruction Manual for Nd: glass Laser, five volumes, KORAD Dept., Santa Monica, California, 1969.

63. U.S. Atomic Energy Commission Report WASH-1295, Status and Objectives of Tokamak Systems for Fusion Research, 1973.

64. Varian Associates, Partial Pressure Gauge Mod 971-0035 and Control Unit Mod 974-0036 Instruction Manual, Vacuum Division, Palo Alto, California, 1966.

65. Wu, L.C., Zilko, J.L., Mukherjees, J.L., Greene, J.E., and Cook, H.E., "Tribology, Chemistry, and Structure of Bias Sputtered TiC Films on Steel Substrates," paper presented International Conference on Wear of Materials, St. Louis, Missouri, 25-28 April 1977.

66. Yuji, E., "Wear Resistance of Vapor Deposited Titanium Carbide Film," Journal of the Japanese Society of Lubrication Engineers, v. 23, no. 21, 1978.

INITIAL DISTRIBUTION LIST

		No. Copies
1.	Defense Technical Information Center Cameron Station Alexandria, Virginia 22314	2
2.	Library, Code 0142 Naval Postgraduate School Monterey, California 93940	2
3.	Department Chairman, Code 61 Department of Physics and Chemistry Naval Postgraduate School Monterey, California 93940	1
4.	Department Chairman, Code 69 Department of Mechanical Engineering Naval Postgraduate School Monterey, California 93940	1
5.	Assoc. Professor F.R. Schwirzke, Code 61Sw Department of Physics and Chemistry Naval Postgraduate School Monterey, California 93940	2
6.	Assoc. Professor K.D. Challenger, Code 69 Department of Mechanical Engineering Naval Postgraduate School Monterey, California 93940	1
7.	LT Michael Thomas Keville, USN 163 W. Genesee St. Chittenango, New York 13037	1
8.	CDR Robert William Lautrup, USN RFD Shawnee, Wyoming 82229	2


ATE
ME